Atmos. Chem. Phys. Discuss., 14, 8633–8693, 2014
www.atmos-chem-phys-discuss.net/14/8633/2014/
doi:10.5194/acpd-14-8633-2014

Atmospheric Chemistry and Physics Discussions

Uncertainties in assessing the environmental impact of amine emissions from a CO_2 capture plant

M. Karl[1], N. Castell[1], D. Simpson[3,4], S. Solberg[1], J. Starrfelt[2], T. Svendby[1], S.-E. Walker[1], and R. F. Wright[2]

[1]Norwegian Institute for Air Research, NILU, Kjeller, Norway
[2]Norwegian Institute for Water Research, NIVA, Gaustadalléen 21, 0349 Oslo, Norway
[3]EMEP MSC-W, Norwegian Meteorological Institute, Oslo, Norway
[4]Dept. Earth and Space Sciences, Chalmers Univ. Technology, Gothenburg, Sweden

Received: 17 December 2013 – Accepted: 17 March 2014 – Published: 31 March 2014

Correspondence to: M. Karl (mka@nilu.no)

Published by Copernicus Publications on behalf of the European Geosciences Union.

Abstract

In this study, a new model framework that couples the atmospheric chemistry transport model system WRF-EMEP and the multimedia fugacity level III model was used to assess the environmental impact of amine emissions to air from post-combustion carbon dioxide capture. The modelling framework was applied to a typical carbon capture plant artificially placed at Mongstad, west coast of Norway. WRF-EMEP enables a detailed treatment of amine chemistry in addition to atmospheric transport and deposition. Deposition fluxes of WRF-EMEP simulations were used as input to the fugacity model in order to derive concentrations of nitramines and nitrosamine in lake water. Predicted concentrations of nitramines and nitrosamines in ground-level air and drinking water were found to be highly sensitive to the description of amine chemistry, especially of the night time chemistry with the nitrate (NO_3) radical. Sensitivity analysis of the fugacity model indicates that catchment characteristics and chemical degradation rates in soil and water are among the important factors controlling the fate of these compounds in lake water. The study shows that realistic emission of commonly used amines result in levels of the sum of nitrosamines and nitramines in ground-level air (0.6–10 $pg\,m^{-3}$) and drinking water (0.04–0.25 $ng\,L^{-1}$) below the current safety guideline for human health enforced by the Norwegian Environmental Directorate. The modelling framework developed in this study can be used to evaluate possible environmental impacts of emissions of amines from post-combustion capture in other regions of the world.

1 Introduction

Post-combustion carbon dioxide capture encompasses the removal of CO_2 from the flue gas of a combustion process, mainly in gas-fired or coal-fired power plants. The most widely used chemical absorption technology for post-combustion on an industrial scale is scrubbing with an aqueous solution of monoethanolamine (MEA, 2-aminoethanol) as a solvent (Rochelle, 2009). In this method, MEA absorbs CO_2

ACPD
14, 8633–8693, 2014

through chemical reaction in the absorber column. Amine-based solvents result in the emission of volatile organic compounds (VOCs) and ammonia (NH_3) to air due to the degradation of the solvent (Strazisar et al., 2003) in the CO_2 capture plant (CCP). The CCP will release amines as gases and liquids to the air, due to volatilisation losses during the absorption process. Estimated emissions of MEA from post-combustion capture are between 0.3 kg and 0.8 kg MEA per tonne CO_2 captured without water-wash (Goff and Rochelle, 2004). Based on concentrations of MEA in the exhaust gas of 1–4 ppmv (Rao and Rubin, 2002), MEA emissions for a full-scale CCP that captures 1 million tonnes CO_2 per year, are expected to range from 40 000 kg to 160 000 kg per year. Recent advances in emission control at CCPs may reduce solvent emissions.

A potential concern for public health is the formation of nitrosamines, nitramines (i.e. N-nitro alkylamines and N-nitro alkanolamines), and amides that are products of the reaction of amines and atmospheric oxidants involving nitrogen oxides (NO_x) under the influence of sunlight (Lee and Wexler, 2013; Nielsen et al., 2012b; Angove et al., 2012; Pitts et al., 1978). Reactions of amines with the atmospheric nitrate (NO_3) radical could be important during night time (Nielsen et al., 2012b) and might lead to the formation of nitramines (Price, 2010). Unlike secondary and tertiary amines, the primary amine MEA does not form a stable nitrosamine in air (Nielsen et al., 2011; Karl et al., 2012). However, the formation of the nitramine of MEA, 2-nitro aminoethanol in the photo-oxidation of MEA has been confirmed (Nielsen et al., 2011; Karl et al., 2012). Richardson et al. (2007) have reviewed the occurrence and carcinogenicity of nitrosamines and nitramines. Nitrosamines are of particular concern, as they have been found to cause tumour formation for approximately 90 % of 300 nitrosamines tested in laboratory animals and bioassays (Låg et al., 2011). Nitramines are also presumed to be carcinogenic, although there are little data available (Låg et al., 2011; Richardson et al., 2007). The possible formation of nitrosamines and nitramines in the plume from post-combustion CO_2 capture systems employing amine-based solvents is the main risk for human health and environment; with implications for designing and implementing this essential technology to mitigate climate change.

ACPD
14, 8633–8693, 2014

The foremost environmental concern associated with amine-based CO_2 capture is the potential risk of nitrosamines in drinking water supplies. Different regulations for nitrosamine and nitramines have been enforced in North America and Europe. The State of California (California EPA, 2006) has an action level of 10 ng L^{-1} for N-nitroso dimethyl amine (NDMA). NDMA is currently not regulated in the United States for drinking water, but has been included in the proposed Unregulated Contaminants Monitoring Rule (UCMR-2; http://www.epa.gov/ogwdw/ucmr/ucmr2/index.html). The US EPA has set a level of 7 ng L^{-1} NDMA in drinking water, representing a 10^{-6} risk for cancer. Canada does not regulate NDMA nationally, but Ontario has established a drinking water quality standard of 9 ng L^{-1} for NDMA. Due to the limited toxicity data on nitramines the Norwegian Institute for Public Health decided to use the NDMA risk estimate for the total concentration of nitrosamines and nitramines in drinking water (Låg et al., 2011). The Norwegian Environmental Directorate (Miljødirektoratet) has directly addressed nitrosamines and nitramines related to amine scrubbing, restricting environmental levels of total nitrosamine and nitramine to 0.3 ng m^{-3} in air and 4 ng L^{-1} in water. The emission permit for the CO_2 Technology Centre Mongstad (TCM) in Norway (de Koeijer et al., 2013) must adhere to these safety limits (Norwegian Climate and Pollution Agency, 2011).

Nitrosamines and nitramines may be formed in the atmosphere after the emissions of precursor amines, but in addition they might also occur in the CCP and be emitted directly to air from post-combustion (Reynolds et al., 2012). In wash water samples of a pilot plant, concentrations of 0.73 µM total N-nitrosamines were found, requiring a ~ 25 000-fold reduction between the wash water unit and downwind drinking water supplies in order to meet the permit limits of the Norwegian Environmental Directorate (Dai et al., 2012). Due to the lack of publicly available data for full-scale CO_2 capture, we have not included direct emission of nitrosamines in our assessment.

While Gaussian-type dispersion models can provide accurate prediction of location and movement of the plume on the local scale, the description of air chemistry in gas phase and aqueous phase leading to the transformation of reactive compounds

ACPD
14, 8633–8693, 2014

is usually highly parameterized or based on semi-empirical schemes for photochemistry (Holmes and Morawska, 2006; Owen et al., 2000). Therefore, we utilized the new framework WRF-EMEP, capable of treating specific air chemistry in addition to atmospheric transport by advection and diffusion. WRF-EMEP is a model system where the meteorological data is generated with the Weather Research and Forecast (WRF) model (Skamarock and Klemp, 2008) and the dispersion and air chemistry is solved with the EMEP model (Simpson et al., 2012). WRF-EMEP was coupled to a multimedia fugacity level III model to simulate annual average concentrations of nitrosamines and nitramines in the water compartment in an evaluative environment.

Karl et al. (2011) made a preliminary evaluation of the impacts of MEA emissions from a hypothetical CCP capturing 1 million tonnes CO_2 per year. The evaluation considered air quality, drinking water and aquatic ecosystems (Karl et al., 2011). However, the uncertainty associated with several of the model parameters and processes affected the results of this assessment; these included branching ratios and rate constants of the amine photo-oxidation scheme, the vertical emission profile, dry and wet deposition, and degradation rates in soil and water.

The goal of the sensitivity analysis presented in this paper is to identify the parameters and processes for which the simulation result, i.e. surface air concentration and total deposition flux of the sum of nitramines and nitrosamines, is most sensitive to. In the present sensitivity analysis, a fictive CCP with generic emissions of amines and NO_x was placed at the location of Mongstad, Norway. Emissions from the CCP were set to 40 000 kg per year MEA and 5000 kg per year diethylamine (DEYA) in all simulations with the WRF-EMEP system, consistent with the amine emissions applied in the study by Karl et al. (2011). The MEA emission amount is a factor of 10–60 higher than in the recent health risk study for the existing TCM facility at Mongstad (de Koeijer et al., 2013). We explicitly allow for the degradation of toxic compounds during transport in air, water and soil, in order to make the assessment more realistic. We also estimate the uncertainties of predicted concentrations of toxic products in ground-level

ACPD
14, 8633–8693, 2014

air and drinking water related to generic amine emissions from a CCP using a range of possible parameterizations in the coupled modelling framework.

2 Methodology

2.1 Model framework

Emission dispersion simulations were performed for a baseline case and several modified cases to estimate the uncertainties due to variations in single parameters. Annual average concentrations of nitrosamines and nitramines in air at ground level and in lake water potentially used as drinking water source were calculated in a 200 km × 200 km domain with Mongstad in the centre. Mongstad (60°48′17″ N; 5°01′50″ E), Norway, is located approximately 60 kilometres north of Bergen. Mongstad is situated at the coastline, only a few meters a.s.l., in the Fensfjorden–Austfjorden which aligns roughly from SE to NW, with steeper terrain and higher hills/mountains on the north side (see topographic map in Fig. 1). The region is influenced by strong westerly winds from the Northern Atlantic for most of the year. To the east, the region is surrounded by a chain of hills and mountains up to 600 m in elevation.

Concentrations calculated by the WRF-EMEP model system were compared to the recommended air and drinking water quality criteria set by the Norwegian environmental authorities. The methodology outlined in the following can be transferred to other world regions and locations where the installation of a CCP is planned. The emission dispersion simulations included the following processes:

1. emission of amines and NO_x from the CCP, represented as a point source (Sect. 2.4).

2. Atmospheric gas phase chemistry of amines, covering oxidation of amines by hydroxyl (OH) radicals and the photolysis of nitrosamines by sunlight (Sect. 2.5).

ACPD
14, 8633–8693, 2014

3. Partitioning of amines, nitrosamines and nitramines to the aqueous phase of clouds (Sect. 2.6).

4. Dry and wet deposition of amines, nitrosamines and nitramines (Sect. 2.6).

5. Fate of nitrosamines and nitramines in soil, transport by runoff to surface waters, and degradation in surface waters. The result was simulation of mean concentrations of nitrosamines and nitramines under steady-state conditions in a generic lake (Sect. 2.3)

Processes 1–4 were implemented into the atmospheric dispersion model, the WRF-EMEP model system (Sect. 2.2). Process 5 was treated by a fugacity level III model (Sect. 2.3) which uses simulated wet plus dry deposition of compounds from the atmospheric dispersion model as input (Fig. 2).

Specific input data to the EMEP model includes (1) dimensions and characteristics of the CCP point source (stack data); (2) emission data per compound; and (3) chemical parameters of the amine photo-oxidation scheme. The chemical data were used to set up the amine chemistry in the EMEP model (Sect. 2.5) and the emission data were used to set up the CCP emission point source (Sect. 2.4). The nested WRF-EMEP model system uses meteorological data predicted by the weather forecast model WRF as input to the EMEP model to calculate air concentrations at the surface (ground-level), and dry and wet deposition of amines, nitrosamines, and nitramines. The deposition (dry and wet) flux of nitrosamines and nitramines is then used as input to the fugacity level III model (Sect. 2.3) which computes mean annual concentrations of nitrosamines and nitramines in the water compartment of a typical lake. Finally, maximum yearly average ground-level air concentration and lake water concentration in the 40 km × 40 km study grid (with Mongstad as centre) inside the inner domain are compared to the pre-defined safety limits, i.e. 0.3 ng m^{-3} in air and 4 ng L^{-1} in drinking water (Låg et al., 2011), respectively, for the sum of nitrosamines and nitramines.

ACPD
14, 8633–8693, 2014

2.2 Description of WRF-EMEP model system

The WRF-EMEP model system combines the WRF numerical weather prediction model (NWP) with the EMEP MSC-W chemical transport model (CTM). This system, which is similar to the EMEP4UK setup (Vieno et al., 2009, 2010), was recently implemented and tested at NILU (Colette et al., 2011; Solberg and Svendby, 2012).

WRF-EMEP follows a nested procedure. It calculates concentrations first in the outer domain (extending from eastern North America to western Europe) with a 50 km horizontal resolution, then uses these as initial and boundary conditions for the intermediate domain (Scandinavia) with 10 km horizontal resolution, and finally uses the outcome from the intermediate domain as initial and boundary conditions for the inner domain (west coast of middle Norway; 200 km × 200 km) with 2 km horizontal resolution. The meteorological data calculated by the WRF model are fed into the EMEP model which is then used to simulate the emission, transport (by advection and turbulent diffusion), photochemical reactions, and dry and wet deposition for each of these nests. Within the setup of this one-way nesting algorithm any air masses that exit the inner domain and then re-enter will have lost the original influence of the inner domain. Atmospheric transport of amines, nitrosamines, and nitramines from the point source were not expected to extend beyond the borders of the intermediate domain (10 km resolution) during the one year calculations. Boundary and initial conditions given by the coarse domain (50 km resolution) were therefore not modified.

As part of the WRF-EMEP model system, meteorological input data (pressure, temperature, wind, humidity, etc.) were generated by the Advanced Research WRF (ARW) modelling system Version 3. The ARW dynamics solver integrates the compressible, non-hydrostatic Euler equations. The equations are formulated using a terrain-following hydrostatic-pressure vertical coordinate (Skamarock et al., 2008). The same vertical configuration as in the EMEP model was employed. WRF offers multiple physics options; we selected those that captured best the precipitation pattern in the complex terrain on the west coast of Norway. The Goddard microphysics scheme with ice, snow

ACPD
14, 8633–8693, 2014

and graupel processes was employed for all the domains. The cumulus parameterization was employed only in the 50 and 10 km domains and the Grell–Deveny ensemble scheme was selected (for details on the schemes see Skamarock et al., 2008). The Mellor–Yamada–Janjic scheme was employed for the parameterization of the planetary boundary layer and the RRTMG scheme for the longwave and shortwave radiation. Initial and boundary conditions for WRF were obtained from the European Centre for Medium-Range Weather Forecasts (ECMWF) global atmospheric reanalysis (Dee et al., 2011) at six hourly intervals with a resolution of 0.75°. Upper-air analysis nudging was employed (FDDA) in the nested domains, and time-varying SST (0.5° resolution) was employed as input to the model, obtained from the NCEP Real-Time SST archives (ftp://polar.ncep.noaa.gov/pub/history/sst).

WRF was also initialized with the NCEP FNL (Final) Operational Global Analysis data given on 1.0° × 1.0° grids prepared operationally every six hours. Results from the comparison of meteorology from WRF initialisations with ECMWF and NCEP FNL data and observations from meteorological stations in the region around Mongstad are presented in Sect. 3.1. In this study we have chosen the meteorological year 2007 for comparability with previous results obtained from the TAPM air quality model (Hurley et al., 2005) presented in the "worst case scenario" study by Karl et al. (2011) for the same area of Norway. Meteorological input variables computed by the WRF model included surface pressure, sea level pressure, geopotential height, potential temperature, temperature at 2 m, sea surface temperature, soil parameters, ice cover, specific humidity, horizontal winds, friction velocity, and surface fluxes of latent heat and sensible heat. Dispersion parameters (boundary layer height, eddy diffusivity, Obukhov length) are calculated in the EMEP model.

The EMEP model is a CTM developed by EMEP Meteorological Synthesizing Centre – West (EMEP MSC-W) at the Norwegian Meteorological Institute. The model has 20 vertical layers in σ-coordinates in a terrain following coordinate system and has generally been used with a 50 km × 50 km horizontal resolution in the EMEP polar stereographic grid. The model top is defined as 100 hPa, and the lowest layer has a depth

ACPD
14, 8633–8693, 2014

of about 90 m. The model has shown to compare very well when evaluated against trace gas measurements of ozone, nitrogen species, and other compounds at rural stations (Jonson et al., 2006; Simpson et al., 2006a, b; Fagerli and Aas, 2008; Aas et al., 2012). We here use open source version rv 4.0 of the EMEP model (released in September 2012), modified for amines and plume-rise for this study. The chemical scheme in the EMEP model (here EmChem09, Simpson et al., 2012) is flexible in the sense that additional compounds and reactions can be included with the help of a chemical pre processor. The chemical equations are solved using the TWOSTEP algorithm (Verwer et al., 1996; Verwer and Simpson, 1995). Anthropogenic emissions of sulphur oxides ($SO_x = SO_2 + SO_4$), nitrogen oxides ($NO_x = NO + NO_2$), ammonia (NH_3), non-methane volatile organic compounds (NMVOC), carbon monoxide (CO), and particulates ($PM_{2.5}$, PM_{10}) are integrated from the TNO-MACC (Kuenen et al., 2011), approximately 7 km × 7 km, emissions to the required 2 km × 2 km. A more detailed description of the gridded emission is given in Sect. S1 in the Supplement. NO_x emissions from the industrial area at Mongstad are given in Table S3. Emissions of the power plant (equipped with a CCP) and NO_x emission from the Mongstad refinery were treated as point sources (Sect. 2.4). Full details of the EMEP MSC-W model are given in Simpson et al. (2012).

2.3 Fugacity level III multimedia model

Fugacity models are routinely applied to investigate the fate of compounds in a multimedia context (Mackay, 2001). The fugacity level III model was used to simulate concentrations of nitrosamines and nitramines in lake water. The model has four bulk media compartments; air, soil, water and sediments. The model includes quantitative advective and diffusive transport processes between these compartments, parameterized with mass transfer coefficients and transport velocities. Loss processes are by advection (e.g. movement of air and water to outside the model domain in addition to permanent removal of sediment) and degradation of the compound. Deposition is assumed to be constant and the steady-state distribution of the compounds is achieved with

ACPD
14, 8633–8693, 2014

equilibrium within the compartments (e.g. between pore-water and sediments), but not between bulk media (i.e. sediment and water have different fugacities). Given a parameterization of the evaluative environment, i.e. area and volume of compartments as well as transport coefficients, there is a linear relationship between deposition/emission and concentration in the water phase for a given compound. Fugacity level III models have successfully been applied to a wide range of compounds and environments (Mackay et al., 1996; MacLeod and Mackay, 1999) and are an integrated part of US EPA's software for environmental fate estimation (US EPA, 2012).

Separate fugacity calculations were made for the nitramine of MEA, the nitramine of DEYA and the nitrosamine of DEYA. The nitramine and nitrosamine of DEYA was approximated with data for dimethylnitramine and NDMA, respectively. The values for physiochemical parameters of these compounds are summarized in Table S1 in the Supplement. The lake water simulations started with the assumption that the deposition to the lake and its catchment was equivalent to that in the 2 km × 2 km grid square with the maximum total deposition for each compound determined by the WRF-EMEP model. Parameters for an exemplary lake, typical for small lakes along the west coast of Norway, are summarized in Table S2. Several of these parameters were varied as part of the sensitivity analyses in this study.

2.4 Point source emissions

Plume rise determines maximum ground-level concentrations from most point sources, as it typically increases the effective stack height by a factor of 2–10 times the actual release height (Hanna et al., 1982). Since maximum ground-level concentration is roughly proportional to the inverse square of the effective stack height, it is clear that plume rise can reduce ground-level concentrations by a factor of as much as 100 (Hanna et al., 1982). Plume-rise calculations for point sources have been included here in the EMEP model. The so-called "NILU-plume" treatment follows the plume rise equations originally presented by Briggs (1969, 1971, 1975).

ACPD
14, 8633–8693, 2014

Inputs to the NILU-plume rise parameterization are the point source characteristics (stack location, height, diameter, exhaust gas temperature and velocity; see Table 1), and boundary layer meteorology characteristics (air temperature, wind speed, friction velocity, Obukhov length scale and mixing height). Plume rise for different boundary layer stability conditions (i.e. unstable, neutral, light stable and stable) is calculated differently where the inverse Obukhov length is used to characterize the boundary layer stability. Point source emissions are injected using a Gaussian distribution centred at the calculated effective emission height to vertically distribute the emissions between the corresponding model layers.

Air temperature and wind-speeds from about 45 m (the WRF-EMEP system's model's lowest layer) are used as approximations for stack-height meteorology. The WRF model also provides friction velocity and Obukhov length data. A fixed surface roughness value of $z_0 = 0.25$ m, adequate for rough surfaces of an industrial area (Wieringa, 1992) was applied. Wind speed u_z at plume height z (m) above ground is calculated as:

$$u_z = u_{z_{\mathrm{ref}}} + \frac{u_*}{\kappa} \int_{v=z_{\mathrm{ref}}}^{v=z} \Phi_{\mathrm{m}}(v, L^{-1}) \mathrm{d}v, \quad (1)$$

where $u_{z_{\mathrm{ref}}}$ is the wind speed at the given reference height (45 m); u_* is the friction velocity; L^{-1} is the inverse of the Obukhov length L; and κ is the Von Kármán constant (0.41). The Monin–Obukhov similarity function Φ_{m} is defined as in Högström (1996). For more details of these, and other recommended schemes, see the final reports from the COST 710 project (Fisher et al., 1998) and Högström (1996). A logic diagram of the "NILU Plume" algorithm to obtain final plume rise is illustrated in Fig. S1 of the Supplement. Two alternative plume rise options were implemented: "ASME Plume" and "PVDI Plume". A description of these two options and a comparison of the final plume rise calculated by the three different methods is presented in Sect. S2 of the Supplement.

ACPD
14, 8633–8693, 2014

Figure 3 shows the difference between the online calculated vertical emission profiles and the constant profile for SNAP category 9 using the CCP stack characteristics. The "NILU Plume" option in WRF-EMEP leads to a vertical emission profile with 65 % in the layer 92–184 m height and 33 % in the layer 184–323 m on average for July 2007. In contrast, a (constant) vertical profile of SNAP category 9 ("Waste treatment and disposal") apportions ca. 35 % of the CCP emissions in the layer 324–552 m. The emission profiles calculated for "ASME Plume" and "PVDI Plume" are very similar. These profiles are comparable to SNAP cat. 9, but 10 % are predicted to be in layers above 552 m height. Among the different plume options, "NILU Plume" has the highest fraction of emissions in the layer 92–184 m as expected due to its generally low plume rise. The online calculated profiles attribute no emissions to the lowest vertical layer in July 2007. The variability of the online calculated profiles is relatively high; the "NILU Plume" July average percentage fraction in the layer 92–184 m varies by ±13 %. A limitation of the current treatment of plume rise from elevated point sources is the relative coarse vertical resolution of the EMEP model, which may lead to inaccurate attribution of emitted material to vertical model layers, in particular in situations with calculated final plume rise of less than 30 m.

2.5 Atmospheric chemical data

The main oxidation pathway in the gas phase is initiated by reaction with the atmospheric hydroxyl (OH) radical (Nielsen et al., 2012b). Among theoretically predicted atmospheric degradation products from the reaction of amines with OH radicals are aldehydes, amides, imines, nitrosamines, and nitramines (Nielsen et al., 2012b). Amines may react equally fast with atmospheric NO_3 radicals during night time; the possibility of the reaction between MEA and NO_3 will be tested in the sensitivity analysis (Sect. 2.7).

Amine chemistry schemes for the OH-initiated oxidation of MEA and DEYA were set based on a simplified photo-oxidation scheme presented by Nielsen et al. (2012a) (Table 2). The schemes consider OH-reaction, photolysis of nitrosamines, reaction of

ACPD
14, 8633–8693, 2014

nitramines with OH, and equilibrium partitioning to the aqueous phase. Rate constants and branching ratios of the MEA and DEYA schemes were adopted from Nielsen et al. (2012b) (Table 2).

In modification to the amine scheme by Nielsen et al. (2012a), the formation of a nitrosamine in the oxidation of MEA was deactivated. Instead the reaction between NO and the N-alkyl radical (RHN·) leads directly to the imine (R=NH) with the rate $k_2 \cdot NO$. Based on quantum chemical calculations there is evidence that the nitrosamine from primary amines, despite forming under atmospheric conditions, is in isomerisation equilibrium with $RNHNOH^+$ which undergoes rapid H-abstraction by O_2 to give the corresponding imine (Tang et al., 2012). For the OH-initiated oxidation of MEA, the nitrosamine was not detected in experiments at the outdoor environment chamber facility EUPHORE (Nielsen et al., 2011; Karl et al., 2012). The modified scheme allows for reaction between the nitramine and OH radicals with rate constant k_6 to form a nitramide ($R(=O)NR'NO_2$).

2.6 Deposition and aqueous phase partitioning

In the atmosphere, amines and their photo-oxidation products are removed by dry and wet deposition processes. Karl et al. (2011) treated dry and wet removal of these compounds in the same way as sulphur dioxide (SO_2) in dispersion simulations using TAPM v.4 (Hurley et al., 2005). In TAPM calculations using the "tracer mode", SO_2 is assumed to be readily dissolved in water and thus totally removed by wet deposition. The efficiency of wet scavenging of amines has been set to 100 % in the TAPM simulations (Karl et al., 2011). In the EMEP model a more realistic approach for the deposition of amines and their products was chosen. Dry deposition and wet deposition characteristics of nitramines and nitrosamines were treated in the same way as for the amines.

Currently, very little is known about the dry deposition behaviour of amines. Since amines are basic substances (MEA: pKa = 9.5) it appears to be more appropriate to treat their dry deposition velocities in the same way as for NH_3. In the EMEP model,

ACPD
14, 8633–8693, 2014

the non-stomatal resistance for NH_3 over vegetated surfaces depends upon surface temperature, relative humidity and the molar acidity ratio, expressed as the concentration ratio of SO_2 to NH_3 (Simpson et al., 2012). Conversely, the canopy conductance of SO_2 is strongly controlled by NH_3 levels, and an operational parameterization was included to take into account co-deposition effects for dry deposition of SO_2.

Parameterisation of the wet deposition processes in the EMEP model includes both in-cloud and below-cloud scavenging of gases and particles (Berge and Jakobsen, 1998; Simpson et al., 2012). By default, the in-cloud scavenging ratio and below-cloud scavenging ratio of nitric acid (HNO_3) was applied for the wet deposition of amines, nitramines and nitrosamines. For most ranges of pH in liquid cloud and rain water, at equilibrium HNO_3 is almost entirely in the condensed phase. Calculations by Ge et al. (2011) demonstrated that for the typical atmospheric liquid water content of fogs and clouds at natural acidity of rainwater (~ pH 5.6) substantial partitioning of amines to the aqueous phase takes place, so HNO_3 appears to be a good model for most amines. We further assumed that wet scavenging of amines, nitrosamines, and nitramines occurs through rain and snow. However, many trace gases that are soluble in cloud or rain drops are insoluble in ice because they tend to be expelled as water freezes or to desorb from the ice surface.

The effect of partitioning of amines to the aqueous phase of clouds is that a smaller fraction of the amine is available for gas phase reaction with OH, and in turn less nitrosamines and nitramines are produced in the gas phase. In cloud droplets, nitrosamines are effectively shielded against photolysis due to the screening effect of dissolved organic compounds (Hutchings et al., 2010). This implies a longer lifetime of nitrosamines in clouds than in dry air. In the parameterization of the aqueous phase chemistry of amines, we assumed that the Henry's law is fulfilled (Hutchings et al., 2010). Phase partitioning equilibrium between gas phase and aqueous phase for amines, nitramines, and nitrosamines according to Henry's Law as listed in Table S5 was implemented into the model. These equilibrium coefficients for the given compounds were consistent with the values used in the fugacity model (Sect. 2.3). In

ACPD
14, 8633–8693, 2014

the EMEP model local cloud fraction, defined in the meteorological input fields, is used as an approximate value for the fractional cloud volume. The fraction of the total (gas + aqueous) mass remaining in the interstitial cloud air (f_g) and the fraction absorbed by cloud droplets (f_{aq}) is calculated as (Simpson et al., 2012):

$$f_{aq} = 1 - f_g = \frac{[C_{aq}]}{[C_T]} = \frac{1}{1 + (HRT\alpha)^{-1}}, \quad (2)$$

where R is the universal gas constant, T is air temperature, H is the Henry's Law coefficient, and α is the volume fraction of liquid cloud water.

2.7 Sensitivity analysis

Karl et al. (2011) identified major uncertainties in the description of processes in the atmosphere and in the environmental fate, due to uncertain atmospheric chemical data, physiochemical properties, and biodegradability. The sensitivity of model results to several of these was explored here. Sensitivity was tested either by variation of a specific parameter, by increasing or decreasing its value by a certain amount compared to the reference value, or by switching off a specific process. The latter was done when the process was considered to be highly uncertain, in particular when the process has not been evaluated by experimental data. In the last three years more studies on the chemical kinetic data of MEA have become available. Hence published chemical data that was associated with the smallest uncertainties was used as a reference value. For test cases with chemical parameters, the actual uncertainty could be larger than the uncertainty based on available literature values, but for practical reasons it was assumed that the uncertainty range of the chemical parameter was covered by the currently published data.

Atmospheric test cases were developed to assess uncertainties in dispersion characteristics, atmospheric chemistry, phase partitioning, and deposition. A summary of the atmospheric cases and the parameter settings of the baseline simulation (case BASE)

ACPD
14, 8633–8693, 2014

and of the cases with parameter variation are given in Table 3. For each sensitivity test, the EMEP model was rerun on 10 km and 2 km domains. Four cases were made to study uncertainties of the MEA chemistry mechanism, including tests on (1) the rate coefficient of the reaction between MEA and OH, k(MEA + OH), (case KOHM); (2) the rate coefficient of the reaction between MEA and NO_3, k(MEA + NO_3), (case KNO3M); (3) the branching ratio for H-abstraction at the NH_2-group in the reaction between MEA and OH (case YIELD); and (4) the rate coefficient between MEA-nitramine and OH, k(MEA−nitramine + OH), (case KNIM). It was assumed that the same products form with the same yield through the NO_3 reaction as through the OH-reaction of MEA. There is experimental and theoretical evidence that NO_3 reaction with primary and secondary amines occurs via H-abstraction (Nielsen et al., 2012b; T. Kurtén, personal communication, 2011). Therefore the assumption on the product spectrum of the MEA + NO_3 reaction appears to be reasonable.

Additional test cases addressed the vertical emission profile and plume dispersion (case PLUME), and the wet removal of MEA and MEA-nitramine (case WDEP). Partitioning to aqueous phase of clouds was tested in one sensitivity test (case AQP), while deactivated in the reference simulation and all other simulations. Uncertainties of the processes related to the secondary amine (i.e. DEYA) were not studied. In order to test how different choices for parameters of the fugacity model affect drinking water concentration, 7 cases were set up. Tested model aspects include lake residence time, soil depth, fraction of carbon in soil and suspended sediment, and degradation rates for nitrosamines and nitramines (Table 4).

3 Results

3.1 Evaluation of WRF meteorology

The WRF-EMEP model used ECMWF met data for the baseline simulation and for the other case simulations. In this work, data from five monitoring stations (Bergen, Fedje,

ACPD
14, 8633–8693, 2014

Flesland, Takle, and Kvamskogen) with temperature, relative humidity and wind speed on an hourly basis have been analysed. Table S6 provides an overview of the meteorological stations located in the wider region around Bergen. The performance of the WRF model was evaluated by comparison of yearly wind roses, daily averages of wind direction, wind speed, and temperature. Two different met data sources – NCEP FNL and ECMWF – were included in the comparison to station monitoring data. Section S3 in the Supplement documents the results of this comparison. Wind roses for 2007 predicted by WRF using ECMWF met data compared well with observation based wind roses (Fig. S2).

Precipitation data for 2007 has been analyzed at 14 stations in the region of Mongstad. Precipitation reached high values in the area of Mongstad, with accumulated monthly values up to 500 mm at the stations of Takle and Mongstad, and 300 mm at Bergen and Flesland. High amounts of precipitation were present during the whole year, June being the only month with a precipitation amount lower than 50 mm. Analysis of the precipitation data on a weekly basis for 2007 showed that the WRF model underestimated the observed precipitation amount at most stations in the study area (Fig. 4). In particular the precipitation peaks in early spring and in fall were not captured by the model. However, the weekly pattern of observed precipitation is well reproduced. Given the general uncertainty associated with modelling precipitation amounts (factor 2–3 or higher) of current state-of-the-art models, the agreement is satisfactory. Some of the stations are extremely difficult to be represented by the model. For instance, Frøyset, the station closest to Mongstad, is situated in the Fensfjorden, which has its own fjord wind system. The agreement between model predicted and observed precipitation was slightly better with ECMWF data than with NCEP FNL data.

The total amount of precipitation for 2007 was above 2000 mm in the coastal parts, and between 3000 and 4000 mm in the mountain parts of the Mongstad region (Fig. S5). Precipitation amount is related to the orography of the landscape, indicating that orographic rainfall is of great importance in the wider region of Bergen. During 2007 the precipitation was between 10–30 % higher than in a normal year, considering

ACPD
14, 8633–8693, 2014

a normal year as the average from 1971 to 2000. Inside the study area, extending 20 km to the East of Mongstad, the WRF model predicts a maximum precipitation amount of ~ 3000 mm (Fig. S4b and c). In the coastal part, precipitation is predicted to be below 1500 mm, lower than the observation-based estimate. Based on comparison of monthly averages it is concluded that the modelled annual precipitation amount in the coastal part is up to a factor 2 lower than observed.

3.2 Evaluation of EMEP model air concentrations

Modelled time series of ground air concentrations of O_3, O_x ($O_x = O_3 + NO_2$), NO and NO_2 were compared to observed data at two air quality monitoring sites Hamna and Leirvåg located in proximity (within a radius of 3 km) of the Mongstad refinery. Figure 5 shows a comparison of O_3, NO and NO_2 air concentrations (as mixing ratios in ppbv) for the time period of 1 January to 30 September 2007 at Hamna station between WRF-EMEP model data and observed data. For ozone concentrations, WRF-EMEP reached good match with observed data at Hamna. Modelled O_3 follows both monthly trends and variations of the monitored time series. Yearly average (2007) modelled NO_2 concentrations at Hamna and Leirvåg were 4.9 $\mu g\,m^{-3}$ and 6.5 $\mu g\,m^{-3}$, respectively, in reasonable agreement with the monitored average concentrations of 7.4 $\mu g\,m^{-3}$ and 4.6 $\mu g\,m^{-3}$, respectively. Modelled peak NO_2 concentrations agree with the monitored peaks, although the timing of the peaks is not exactly reproduced. In the spring months (March–April) modelled NO_2 was lower than the observed data. In the summer months (June–August) the agreement between modelled and observed NO_2 was better, showing that WRF-EMEP is capable of reproducing the photochemical reactivity at Mongstad. Yearly average (2007) modelled NO concentration at Hamna was 0.65 $\mu g\,m^{-3}$ (~ 0.5 ppbv). Modelled NO concentrations were in general lower than monitored data. Due to the titration effect, it is extremely difficult to simulate NO and NO_2 concentrations close to the emission source (Mongstad refinery). It is therefore preferable to compare the sum of O_3 and NO_2 concentrations. Observed concentration of O_x

ACPD
14, 8633–8693, 2014

is reproduced quite well by the WRF-EMEP model, both in terms of absolute values and in terms of variability. Also the monthly trends matches.

The good match with ozone observations is important for the simulation of amine degradation, since ozone is the main photochemical precursor of OH radicals. Modelled OH concentration at Hamna station in July reached a midday maximum of $\sim 1.2 \times 10^7$ molecules cm^{-3} (Fig. 6a). The 24 h averaged OH concentration was 2.6×10^6 molecules cm^{-3}; in good agreement with previous model simulations for the Mongstad region employing the model COSMO/MUSCAT (Wolke et al., 2004) presented in the report by Nielsen et al. (2012a). Modelled MEA concentrations at Hamna station revealed peak concentrations of > 100 ng m^{-3} on several days in July (Fig. 6a), when Hamna station was downwind the CCP at Mongstad receiving the plume containing high amine and NO_x concentrations. The peaks were associated with low plume rise and injection of > 90 % of the amine emissions into the second model layer (92–184 m). Enhanced MEA concentrations were frequently concurrent with suppressed OH concentrations, probably due to high NO_2 in the plume. The vertical resolution of the model with the lowest level of ca. 90 m height has strong implications for the modelled MEA ground-level concentrations. However, the timescale for vertical mixing in the unstable boundary layer is typically much less than the chemical lifetime of MEA in the reaction with OH radicals (ca. 1–2 h during daytime at Mongstad). We therefore expect that the relatively coarse vertical resolution of the EMEP model is adequate for the simulation of amines, especially since we are mainly interested in yearly average concentrations.

3.3 Evaluation of atmospheric production yields

In order to evaluate the modelled atmospheric production yield of nitramines in WRF-EMEP, the reference simulation included emissions of a chemically inert compound (passive tracer) with the same emission rate as MEA. Deposition and chemical reaction of nitramines was deactivated in this test run. The difference between the air concentration surface fields of the reactive amine and the inert tracer provides an estimate of the

ACPD
14, 8633–8693, 2014

amine amount that reacted with OH. The maximum of the reacted amine was at a distance of about 5–6 km to the West of the CCP Mongstad, computed as concentration difference of 0.39 ng m^{-3}. The corresponding air concentration of MEA at the location of the maximum reactivity was 24.8 ng m^{-3}. Thus only 1.6 % of MEA was degraded by OH-reaction at the location. Closer to Mongstad high NO_2 concentrations led to a reduced production of OH radicals and hence less photochemical reactivity of the amine. The corresponding modelled air concentration of the MEA-nitramine – produced in the OH-reaction of MEA – was 4×10^{-3} ng m^{-3}. The spatial correlation between the reactivity of MEA and the MEA-nitramine concentration (Fig. 6b), confirms the capability of the model to reliably predict the photochemical production of the nitramine.

The apparent yield of nitramine was calculated as the ratio of nitramine produced to MEA reacted and was found to be 0.87 %. This is within the range of estimated nitramine yields for the OH-reaction of MEA reported by Nielsen et al. (2011). Apparent product yields of MEA-nitramine in photo-oxidation experiments in the large photo reactor facility EUPHORE were 0.3 % to 1.5 % depending on the NO_x-level in the experiment. For urban regions predicted MEA-nitramine yields ranged between 0.3 to 1.0 % and for rural regions ranged between 0.005 and 0.3 % (Nielsen et al., 2011). A reason for the higher nitramine yield calculated from WRF-EMEP might be that the reaction between MEA-nitramine and OH radicals was not considered in the test, while it constitutes a relevant loss path of the nitramine in chamber experiments. Modelled NO_2 yearly average air concentrations in the area around the maximum photochemical production were 4–5 µg m^{-3} (2.5–3.5 ppbv). The area can be described as moderately polluted.

3.4 Results of the simulations

Yearly average surface air concentrations and accumulated total deposition of the sum of nitrosamines and nitramines calculated for the different parameter variation cases were compared for the study grid of 40 km × 40 km with the CCP in the centre. Wet and dry deposition of nitrosamines and nitramines was used to drive the fugacity model to

ACPD
14, 8633–8693, 2014

compute average concentrations of nitrosamines and nitramines in the water compartment. Based on the maximum total deposition fluxes of the sum of nitrosamine and nitramines inside the study area, a worst case for the atmospheric fate of MEA and DEYA was set up, by using the parameter choice which resulted in the higher deposition flux when comparing the respective simulation case to the baseline case. Correspondingly, a second worst case was set up for the soil-water-sediment fate, based on the respective parameter value choices that gave the higher drinking water concentration in the standard lake. Table 5 summarizes the parameter value choices for the worst cases addressing atmospheric fate and soil-water-sediment fate, together with the respective baseline cases.

While the response to a change of chemical parameters results in a clear response of the resulting air concentration, a change of the plume rise parameterization also causes a change in the spatial pattern. To test if the selected parameter choice for the worst case (Table 5) gives the highest concentration, the worst case was also run with "PVDI Plume" (replacing "NILU Plume").

The spatial distribution of annual average air concentration of amines (MEA + DEYA) at ground level was similar for all simulations that used the plume rise parameterization "NILU Plume", with a first maximum in the grid cell of the CCP plant, and a second somewhat lower maximum about 4 km Northwest of Mongstad (Fig. 7a). Maximum surface concentration of amines was 65 ng m^{-3} in the baseline run. Increasing the rate constant of the MEA + OH reaction (case KOHM) by 21 % had a negligible effect (< 0.2 %) on the maximum surface concentration. Similarly, the additional reaction of MEA and NO_3 (case KNO3M) did not affect the surface concentration pattern of amines. Using the wet scavenging rate of SO_2 instead of HNO_3 to describe the wet deposition of MEA (case WDEP) increased the maximum concentration slightly, by 0.9 %. The largest change of the maximum concentration was found when a different plume rise parameterization was applied. Maximum surface concentration of amines was only 26 ng m^{-3} when using the "PVDI Plume" option (case PLUME; Fig. 7b), a reduction by 60 % compared to the baseline case. The "PVDI Plume" option entails a higher final

ACPD
14, 8633–8693, 2014

plume rise, leading to lower surface concentrations in the vicinity of the CCP. The final plume rise for the stack configuration of this study (60 m high stack, diameter of 7 m, and exit velocity of 10 m s^{-1}) calculated by "PVDI Plume" may be 2–3 times larger than the final plume rise calculated by "NILU Plume" for stable and unstable conditions. Maximum ground level concentration decreases roughly proportional to the square of the effective emission height; thus an increase of the effective emission height from about 140 m to about 300 m – due to a 3 times larger final plume rise – could potentially cause a reduction of the maximum concentration by up to 72 %. The spatial distribution and maximum concentrations in the worst case using the "PVDI Plume" option were quite similar to the case PLUME, indicating that the local dispersion of emitted amines is mainly determined by the applied plume rise parameterization.

Figure S6 in the Supplement shows the annual average air concentration of the sum of nitrosamines and nitramines, produced in the photochemical reactions of MEA and DEYA. In the maximum impact area, MEA-nitramine, DEYA-nitramine, and DEYA-nitrosamine contributed 78 %, 14 %, and 7 %, respectively, to the sum concentration (baseline case). The reacted amount of MEA in the different cases was quantified in terms of concentration difference (in ng m^{-3}) between the chemically reactive MEA model species and a chemically inert, passive tracer, emitted with the same rate and yearly amount as MEA. The reacted amount of 0.18 ng m^{-3} in the baseline case is only 0.3 % of the maximum air concentration of MEA; thus chemical degradation has a marginal effect on the ground-level concentration of the amine in the vicinity of the CCP, as discussed above. July was the month with the highest photochemical activity in 2007 and the reacted amount of MEA was up to 2.0 ng m^{-3} in this month, dominating the annual average. Figure S7 gives an overview of the spatial pattern of the reacted amount of MEA in the various cases.

In the baseline case and in the cases which use the plume rise option "NILU Plume", the maximum surface air concentration of the sum of toxic products was located close to the CCP at a distance of 4 km to the west. The impacted area was about 20 km long and 10 km wide in a SE–NW direction due to dominant E–SE winds during the

ACPD
14, 8633–8693, 2014

photochemical active period in July. From the CCP Mongstad stack, pollutants are injected into the second and third vertical layer of the EMEP model and presumably the plume is transported in these layers. In the third layer (184–324 m) at Mongstad, the winds from W to SW had a somewhat higher frequency (15 % of the time) than the winds from SE (7–12 % of the time; Fig. S8), but winds from E–SE directions had frequently high wind speeds in July. Case KNO3M involves the additional reaction of MEA with NO_3 radicals using a rate constant of 1.5×10^{-13} cm^3 $molecule^{-1}$ s^-1. Compared to other sensitivity cases, the case KNO3M had the highest reacted amount of MEA, 0.38 $ng\,m^{-3}$. Reaction with NO_3 occurs mainly during night time resulting in a more uniform distribution of the sum of nitrosamines and nitramines (Fig. S6d), and a wider area with enhanced chemical turnover, extending from Mongstad to about 10 km NW of the CCP. The NO_3 reaction is relevant during most months of the year. The dispersion pattern of KNO3M is therefore impacted by the frequency of different wind directions on the yearly average.

In case PLUME which applies the plume rise parameterization "PVDI Plume" MEA is injected into higher vertical layers and therefore the reacted amount in the vicinity of the CCP becomes negligible. Case PLUME showed the maximum impact area located 15–20 km SE of the CCP (Fig. S6b) and had the lowest maximum concentration of nitrosamines and nitramines. The main effect of the higher plume rise is the transport of emitted compounds out of the study area, effectively reducing the impact in the vicinity of the CCP. In the worst case where additional NO_3 reaction is combined with the "NILU Plume" option (Fig. S6i) the main area of impact extends from Mongstad to about 20 km NW of the CCP. In this area, the reacted amount of MEA is about two times higher than the maximum reacted amount in the baseline case. The increased impact is mainly a result of the relative high NO_3 reactivity in late autumn and winter. The worst case run using "PVDI Plume" instead of "NILU Plume" resulted in a similar pattern but with on average ~ 50 % smaller air concentrations of the sum of nitrosamines and nitramines (Fig. S6j).

ACPD
14, 8633–8693, 2014

Table 6 provides an overview of the maximum air ground level concentrations of amines and toxic gas-phase products. Maximum values of the sum of nitrosamines and nitramines in the sensitivity test range from 0.6 to 6.5 pg m^{-3}, with the highest modelled concentrations in case YIELD in which the branching ratio k_{1a}/k_1 of the H-abstraction at the NH_2-group of the MEA molecule is doubled compared to the reference. Increasing the rate constant of the MEA + OH reaction by 21 % (case KOHM) increased the maximum reacted amount and also the maximum concentration of MEA-nitramine almost linearly, by 19 %. The maximum sum concentration of nitrosamines and nitramines increased only by 15 %, since DEYA-nitramine and DEYA-nitrosamine production did not change. Case AQP which takes into account equilibrium partitioning of MEA to the aqueous phase shows lowest maximum of the reacted amount for the studied cases, and a decrease of the sum of toxic oxidation products by 62 % compared to the baseline case. Partitioning of MEA to the aqueous phase of low clouds effectively reduces photochemical production of nitrosamines and nitramines, because it reduces the fraction of MEA in the gas phase, available for reaction with OH.

Dry deposition contributed on average 40 % to the total deposition of the sum of nitrosamines and nitramines inside the study grid. The relatively large contribution of dry deposition is in contrast to results from the "worst case scenario" study by Karl et al. (2011) who reported that the annual grid-averaged dry deposition flux of nitrosamines and nitramines was only about 1/8 of the annual wet deposition flux. The more important role of dry deposition in the present study is probably due to a more advanced description of the dry deposition process and less frequent precipitation in the WRF-EMEP model system, as will be discussed in Sect. 3.7. In general, the location of the maximum deposition impact was found within 5 km distance of the CCP for the parameter variation cases where the total deposition maximum was dominated by dry removal, whereas it was found in the region 15–20 km E to NE of the CCP for the cases where the total deposition maximum was dominated by wet removal. In the baseline case, dry deposition contributed 70 % to the total deposition at the maximum impact location.

ACPD
14, 8633–8693, 2014

In the photochemical active month of July 2007, the model predicted amount of rain was highest (ca. 240–310 mm) at the chain of hills and mountains ca. 15 km to the east of Mongstad. In all simulated cases, the maximum impact from wet deposition occurred in the region 15–20 km E to NE of the CCP. Since this receptor region, the eastern part of the Fensfjorden–Austfjorden and the Masfjorden, is downwind of the CCP frequently during summer when W to NW winds are common, it can be expected that this is the highest impact area for wet deposition of nitrosamines and nitramines that form in the photo-oxidation of emitted amines. In the worst case, maximum annual deposition flux of the sum of nitrosamines and nitramines reached values of up to 3.8 $\mu g\,m^{-2}\,yr^{-1}$; about three times higher than in the baseline case (Fig. 8). Dry deposition contributed 70 % to the deposition maximum located in close vicinity to the plant. When the plume rise parameterization "PVDI Plume" was used in the worst case, the resulting deposition maximum (3.3 $\mu g\,m^{-2}\,yr^{-1}$) was located approximately 15 km east of the plant (Fig. 8e), where dry deposition contributed only 9 %. The location of the maximum impact critically depends both on the description of the plume rise and of the dry/wet removal in the model.

The largest increase in a test case with variation of a single parameter was found for YIELD (Fig. 8f) with an increase of the deposition flux of the sum of nitrosamines and nitramines by 80 % compared to the baseline case; this is due to a doubling of the branching ratio k_{1a}/k_1. Use of the wet scavenging rates of SO_2 instead of the scavenging rates of HNO_3 (WDEP) reduced the wet deposition flux by almost 70 %. In the EMEP model, the scavenging ratios of SO_2 for both in-cloud and below-cloud scavenging are 1/5 of the scavenging ratios of HNO_3. In WDEP, dry deposition was more important than wet deposition and the maximum of total deposition (1.08 $\mu g\,m^{-2}\,yr^{-1}$) was close to the plant (Fig. 8g).

Table 7 shows the effect on sum nitrosamine and nitramine when varying the selected parameters in the fugacity model. As expected the hydrology of the system, here exemplified by the residence time of the water, has a large impact on the predicted concentrations. Varying the depth of the lake and the area has a similar effect

ACPD
14, 8633–8693, 2014

on residence time and therefore also on concentrations in the water. Perhaps somewhat surprising is the negligible effect of changing the carbon content of both the soil and the sediment compartment in the system.

On the other hand, increasing the depth of the soil itself leads to a lower concentration of the compounds in the lake, since more of the contaminants will be "stored" in the soil compartment. The explanation why the soil chemistry is not important, but the soil depth is, lies in the fact that most of the compound's amount is associated with water, and increasing the depth of the soil also increases the volume of water in the soil compartment of the model. Increasing the degradation rates of the contaminants reduces the concentrations in the lake as expected. The sensitivity of the model parameters indicate that efforts should be made to have as accurate numbers as possible for the physical characteristics of the catchment and the degradation rates of the compounds.

3.5 Mass balance of MEA

The atmospheric MEA mass balance in the 200 km × 200 km inner domain from the WRF-EMEP simulation for year 2007 was inspected in the baseline case. About half of the emitted amount of MEA (40 000 kg) was transported out of the inner domain by diffusion and advection (19 800 kg). Net transport out of the inner domain represented the major removal pathway of MEA. Recirculation of MEA from the intermediate domain (10 km resolution), re-entering the inner domain, corresponded to about 2 % of the total emitted amount. Dry deposition and wet deposition were both relevant for the removal, and contributed 29 % and 17 %, respectively. The loss of MEA by reaction with OH radicals contributed only 5 % (~ 2100 kg). The relatively small contribution of chemical degradation also explains why ground level MEA concentrations were not sensitive to a change of the rate constant by 21 %. On the other hand, production of MEA-nitramine increased almost linearly with the increasing MEA + OH rate constant. The majority of the chemical turnover in the MEA + OH reaction leads to the production of carbonylic products, which are not further studied here.

ACPD
14, 8633–8693, 2014

3.6 Removal of nitramines and nitrosamines

Reducing the rate constant of the reaction between MEA-nitramine and OH by a factor of 23 had a negligible effect on the sum concentration (see Table 6), indicating that the removal of nitramines by OH-reaction is not a relevant loss process in the 40 km × 40 km study grid. However, analysis of the atmospheric loss pathways of the sum of nitrosamines and nitramines in the total inner domain (200 km × 200 km) revealed that chemical degradation constituted 21 % of the total loss in the atmosphere (Fig. 9a). Due to the large contribution of MEA-nitramine to the sum of nitrosamines and nitramines in the atmosphere, the reaction of MEA-nitramine is the most relevant loss reaction of the sum of toxic products. DEYA-nitrosamine, which is lost rapidly by photolysis in sunlight, certainly has a higher fractional loss by chemical degradation, but its contribution to the atmospheric sum concentration was minor. Net transport of nitrosamines and nitramines out of the inner domain contributed another 20 % to the total loss. Dry and wet deposition were equally important removal processes, each contributing one third to the total loss.

Degradation of nitrosamines and nitramines in water was the dominant removal pathway for these compounds (Fig. 9b) in a generic lake receiving maximum deposition flux (dry and wet). Minor loss processes were run-off (10 % of total loss) and degradation in soil (15 % of total loss). Partitioning of nitrosamines and nitramines to sediments was negligible.

3.7 Comparison with TAPM simulation results

Monthly average air concentration, dry deposition and wet deposition of an inert tracer emitted from the CCP with a unity emission rate (1 g s^{-1}) from the baseline case with the WRF-EMEP model system were compared to results of the previous "worst case scenario" study using the TAPM model (Karl et al., 2011). The comparison is summarized in Table S4 in the Supplement. Maximum monthly mean air concentration was in a range of 20–140 ng m^{-3} and 30–140 ng m^{-3} for WRF-EMEP and TAPM, respectively,

ACPD
14, 8633–8693, 2014

in the 40 km × 40 km study area. Yearly average air concentrations showed a similar spatial distribution with a centre 5–10 km N–NW of the CCP, and a second centre 5–10 km SE of the CCP (Fig. S9), indicating that dispersion by the main wind direction on a yearly average was reproduced in a similar way. The TAPM simulation had a wider impact area with concentrations > 10 ng m^{-3} and a lower maximum (30 ng m^{-3} instead of 45 ng m^{-3}) probably due to a higher plume rise. The first vertical layer, from which ground-level concentrations were taken, is ca. 90 m in the EMEP model while it is only 10 m in TAPM.

Maximum monthly dry deposition of the inert tracer was in the range of 0.9–4.8 mg m^{-2} and 0.1–1.1 mg m^{-2} for WRF-EMEP and TAPM, respectively, with on average 7 times higher values in the WRF-EMEP simulation. In general, the dry deposition maximum simulated by WRF-EMEP is centred close to the CCP and shows a similar spatial distribution as the mean air concentration. TAPM results for dry deposition show a maximum at a distance of 20 km E of the CCP in the mountains. Maximum monthly wet deposition flux was in the range of 0.4–2.2 mg m^{-2} and 2.2–6.0 mg m^{-2} for WRF-EMEP and TAPM, respectively, with on average 3 times lower values in the WRF-EMEP simulation. The wet deposition maximum simulated by WRF-EMEP is located very close to the CCP, while the maximum simulated by TAPM is ca. 20 km to the East in the mountains. Total precipitation amounts simulated by TAPM were as much as twice as high as amounts observed in the mountains. We therefore considered the wet deposition maximum in the mountains computed by TAPM not to be reliable. On the other hand TAPM results showed a maximum area ca. 5 km NE of the CCP, where predicted precipitation agreed with station observations. For the comparison, maximum values were only taken from the area closer to the plant.

Possible reasons for the location of maximum dry deposition and wet deposition fluxes of the inert tracer at 20–30 km distance E of the CCP as simulated by the TAPM model – compared to the much closer location in the WRF-EMEP model – include the obviously too high frequency and amount of precipitation in the mountains in the TAPM simulation; different underlying land use information, different treatment of scavenging

ACPD
14, 8633–8693, 2014

by dry and wet deposition, and different vertical stratification of the models. In the TAPM simulation, the Lagrangian plume sub grid model was applied in order to account for near-source effects, including gradual plume rise and near-source dispersion. Deposition processes in the TAPM model were treated on the Eulerian grid, while they were neglected in the sub grid model.

3.8 Meteorological data source

Dispersion of emitted amines in the baseline case showed little change when the meteorological data from NCEP FNL was applied as expected due to the high similarity of the annual wind roses obtained from WRF model runs with ECMWF and NCEP FNL meteorology (Fig. S2a–c). Maximum modelled surface concentration of amines from the baseline case run with NCEP FNL met data in the study area (62 ng m^{-3}), was located at the same place as in the run with ECMWF data. However the impact area of toxic gas phase products was different. In the calculation with NCEP FNL, the impacted area was found 10–20 km NE of the CCP, with a maximum concentration for the sum of nitrosamines and nitramines close to 1 pg m^{-3} (Fig. S6k). The reason for the different impact area, compared to the baseline case run with ECMWF data, might be differences in the prevailing wind direction during the photochemical active month July, with more frequent SW winds in the NCEP FNL met data (Fig. S2f vs. S2e). Maximum wet deposition flux of the sum of nitrosamines and nitramines was 1.04 µg m^{-2} yr^{-1} when using NCEP FNL met data (Fig. 8h), only slightly higher than in the baseline case with ECMWF met data. As in the other modelled cases, the maximum impact from wet deposition occurred in the region 15–20 km E–NE of the CCP. Predicted precipitation amount for July in this area was between 150 and 250 mm. Brekke is the met station closest to this impact area. Precipitation amount time series at Brekke simulated using ECMWF met data is in quite close agreement with the observed time series in summer, while the simulation using NCEP FNL underestimates the observed amounts by ca. 50–80 % (Fig. 4). In simulations with the two met datasets for July, the hills and

ACPD
14, 8633–8693, 2014

mountains along the Eastern part of the Fensfjorden–Austfjorden and the Masfjorden received the highest precipitation amounts (up to 380 mm) inside the study area.

4 Discussion

The performance of the WRF-EMEP model system for use as a tool for impact assessment of amine emission from post-combustion capture was evaluated in this study. We applied the new modelling framework to a hypothetical CCP located at Mongstad, west coast of Norway, as a case study. Temperature and frequencies of wind direction and wind speed predicted by the WRF model using ECMWF data were in good agreement with observations from meteorological stations in the region. Fast small-scale variations of the observed NO_2 concentration at Mongstad were not captured by the EMEP model. Observed NO_2 peaks were likely a result of short-term variation in the local emissions from the industrial area, which is not represented in the model. Plume rise from the CCP point source was implemented into the EMEP model for calculation of the vertical emission profile of amines online with the local meteorology. However, accurate treatment of injection height is limited by the relative coarse vertical resolution of the EMEP model. A refinement of the vertical structure of the EMEP model is currently under development.

A condensed atmospheric reaction scheme for amines – leading to the production of nitrosamines and nitramines – was included in the EMEP model, for the first time allowing for prediction of time dependent concentrations of nitrosamines and nitramines in air and deposition. The study showed that amine emissions were spread over a relatively wide region. The particle formation potential of CCP amine emission was not assessed. Losses of gas-phase alkanol amines due to formation of low-vapour pressure amine salts might be significant, in particular close to point sources (Nielsen et al., 2012b). For example, alkyl aminium nitrates exhibit comparable stability to that of ammonium nitrate under atmospheric conditions (Salo et al., 2011). However, the impact of gas-to-particle conversion of the emitted amines is difficult to quantify because it

ACPD
14, 8633–8693, 2014

depends on the magnitude of sources and sinks of the acids (e.g. nitric acid), the amounts of other amines or ammonia present that compete for available acids, and the amine salt equilibrium constants which are not known for many amines.

A fugacity level III model was coupled to the EMEP model in offline mode to simulate the steady-state distribution of nitrosamines and nitramines in an evaluative environment. We opted to use a generic catchment structure to arrive at likely concentrations of the contaminants in sources for drinking water since a more detailed local analysis would require a large amount of more precise measurement of physical and chemical characteristics of a chosen focal catchment. Though fairly advanced methods for sensitivity and uncertainty estimation exist for fugacity models (see e.g. MacLeod et al., 2002; Saloranta et al., 2007), they require measurements of the studied compounds in the environment (after exposure) and sufficient amount of environmental data to calibrate the models. Both requirements are not fulfilled in the current context.

The orographic rainfall when humid Atlantic air meets the hill chain in the east of Mongstad is difficult to predict with numerical models. The WRF model driven by ECMWF meteorology copes quite well with this situation and the West–East gradient of precipitation amount is reproduced in a realistic manner. However, the average precipitation amount, and the rainfall frequency in July over the flat terrain in the coastal area around Mongstad, is underestimated by WRF. Increasing the precipitation amount, but not the frequency, would lead to dilution of the compounds and proportionally decreasing their concentration in wet deposition. Higher precipitation frequency along the trajectory from the CCP to the east would result in an impact area closer to the CCP, but since – on the yearly average – the time scale for chemical reaction of the amine (about 3 h) is longer than the time scale for transport (less than 1 h), the maximum wet deposition would decrease. On the other hand, applying a more realistic precipitation frequency in July everywhere in the coastal part of the study area could increase wet deposition flux in the vicinity of the plant by a factor of 2–3. We conclude that the computed deposition fluxes of the sum of nitrosamines and nitramines have an additional

ACPD
14, 8633–8693, 2014

uncertainty of a factor of two due to underestimated frequency and amount of precipitation.

The "worst case scenario" by Karl et al. (2011) aimed at the estimation of maximum tolerable amine emission from post-combustion in order to avoid adverse effects on aquatic environments and human health according to the precautionary principle. This involved several conservative assumptions about the environmental fate of amines and their oxidation products, such as instant conversion of emitted amines into nitramines and nitrosamines, and the non-degradability of the toxic compounds in air, water and soil. Karl et al. (2011) applied a constant conversion yield of 1 % of the total emitted amine (MEA) amount implying that MEA-nitramine was directly emitted from the CCP stack. Based on this, the calculated maximum yearly deposition flux of MEA-nitramine was 460 $\mu g\,m^{-2}$. For comparison, the calculated total conversion yield for the WRF-EMEP simulation was 0.015 %, about 1/70 of the worst case conversion. Dividing the worst case deposition of 460 $\mu g\,m^{-2}$ by 70 results in a deposition flux of 6.6 $\mu g\,m^{-2}$; a factor of 1.7 higher than the deposition (3.8 $\mu g\,m^{-2}$) in the current atmospheric worst case using WRF-EMEP. In total, the modelled deposition flux maximum is about 1/120 of the previous estimate by Karl et al. (2011), mainly due to detailed treatment of the production of MEA-nitramine in the atmospheric oxidation of MEA and the lower rainfall amount and frequency in the WRF-EMEP model system.

Steady-state drinking water concentration of the sum of nitrosamines and nitramines determined by the fugacity model considers degradation of these compounds in soil and water. Loss by run-off is only 10 % in the present study, implying a 10 times longer retention time in the lake than in the study by Karl et al. (2011). Increased retention time in turn leads to increased degradation of the compounds in lake water. The drinking water concentration in the current worst case is roughly 10 times lower than the MEA-nitramine drinking water concentration calculated in the study by Karl et al. (2011), which did not consider degradation in soil and water.

In a recent study by de Koeijer et al. (2013) on the health risk of amine emissions to air from the TCM (CO_2 Technology Centre Mongstad) plant, an attempt was made to

ACPD
14, 8633–8693, 2014

include a simplified treatment of amine chemistry by calculating the average chemical conversion along the trajectory of maximum concentrations from plant to area of maximum impact. In that study a constant yield of less than 0.3 % for MEA-nitramine in the reaction of MEA with OH was used. The conversion applied by de Koeijer et al. (2013) is thus at most 1/3 of the conversion as computed by WRF-EMEP model system, which takes into account the spatial and temporal variability of levels of OH, NO, and NO_2.

Additional sources of nitrosamines and nitramines, such as the direct emission of these compounds from the CCP were not considered in this study. Reliable estimates on the amount of nitrosamines directly emitted to atmosphere are necessary to enable the environmental impact assessment of commercial scale post-combustion (Reynolds et al., 2012). Actual human and environmental exposures to nitrosamines and nitramines are likely to be higher than estimated here due to natural background levels. In a baseline study for TCM, background air concentrations of 5–30 $ng\,m^{-3}$ of dimethylamine were reported (Tønnesen et al., 2011). The corresponding nitrosamine, NDMA, was not found in the air samples above the detection limit of the method ($10\,pg\,m^{-3}$). We expect that further improvement of the analytical methods for determination of nitrosamines and nitramines in air will reveal measurable concentrations. Measurements of amines in the plume and surroundings of an operative CCP are essential for the further evaluation of the WRF-EMEP system.

Degradation rates for nitrosamines and nitramines in soil and water are poorly known, yet the sensitivity trials show that the values chosen for these have a strong influence on the simulated final concentrations of these compounds in the lake water. Several studies investigated the degradation rates of various nitrosamines in soils, in conjunction with use of wastewaters treated with chloro-compounds for recharge or irrigation purposes (Kaplan and Kaplan, 1985; Zhou et al., 2005; Yang et al., 2005; Drewes et al., 2006). The results from these and other studies indicate half-lives of 1–22 days, with microbial activity being the dominant mechanism for degradation. In surface waters, photo-oxidation of nitrosamines is an important mechanism, while microbial activity appears to be less important (Plumlee and Reinhard, 2007). Yang et al.

ACPD
14, 8633–8693, 2014

(2005) conclude that NDMA will have longer persistence and increased leaching in soils in areas with sparse vegetation, low organic matter content and thus limited microbial activity. Such soils are typical for the Mongstad area of our study.

Consideration of amine oxidation by NO_3 radicals increased maximum surface concentration of the sum of nitrosamines and nitramines by 150 % in our simulations. NO_3 is the predominant nocturnal oxidant and the NO_3 reaction takes place throughout the year, leading to a more uniform spatial distribution. Only few smog chamber studies looked into the kinetics and products from NO_3 oxidation (Malloy et al., 2009) and amine reactions with NO_3 are not well understood (Price, 2010). Based on PTR-MS detection of gas phase compounds of the reaction between secondary aliphatic amines and the NO_3 radical, Price (2010) proposed the formation of nitramines by H-abstraction at the NH-group and subsequent reaction of the resulting N-amino radical with NO_2 to explain high abundance of nitramines in the experiments.

5 Conclusions

The WRF-EMEP model system, which combines the WRF numerical weather prediction model with the EMEP MSC-W chemical transport model, was modified to include treatment of atmospheric chemistry of amines and plume-rise to address uncertainties in the environmental impact assessment of post-combustion CO_2 capture with amine technology. The meteorological data of air temperature, wind speed and wind direction calculated by the WRF model on 2 km horizontal resolution compared well with observed met data in the region of Bergen at the West coast of Norway. Frequency and amount of precipitation due to orographic rain at the mountain chain ca. 10–20 km east of Mongstad was underestimated by the WRF model, causing an additional uncertainty of modelled deposition fluxes of nitrosamines and nitramines by a factor of two. It was beyond the scope of this work to study the impact of the year-to-year variation of meteorology; however the selected baseline year 2007 is rather representative for the meteorological conditions of the region.

ACPD
14, 8633–8693, 2014

WRF-EMEP reproduced the photochemical reactivity in the atmosphere which is of prime importance for the simulation of amine degradation by OH radicals. Modelled summertime 24 h OH concentration average was in good agreement with previous box model studies and the atmospheric production yield of MEA-nitramine was in the range reported from photo-oxidation experiments in EUPHORE. Future modifications of the EMEP model should take into account particle formation from amines, as this might be a significant loss process close to the point source. The sensitivity analysis of the EMEP model strongly suggests that oxidation of amines by NO_3 radicals is of importance. Currently only one study (Price, 2010) has qualitatively addressed nitramine formation in the oxidation of amines by NO_3 radicals.

The location of the maximum deposition impact from the plant showed considerable spatial variability, depending on the treatment of plume rise, characterisation of dry and wet deposition, and the meteorological input data on wind speed and direction. The scavenging properties of amines have not been studied, but the use of NH_3 to represent dry removal and the use of HNO_3 to represent wet removal in the EMEP model appears to be plausible approximation. In contrast to the highly soluble nitrosamines and nitramines forming in the oxidation of alkanolamine, the solubility of the analogous alkyl compounds may be limited due to their lower Henry's Law constants. Dry removal of nitrosamines and nitramines has been neglected in previous environmental impact assessments and more research on the scavenging properties of these compounds is needed.

The fugacity level III model is a useful tool for quantifying the fate of a substance and for predicting concentrations to which organisms, including humans, are exposed. Our sensitivity analysis of the fugacity model indicates that catchment characteristics and chemical degradation rates are among the important factors for determining concentrations of nitramines and nitrosamines (Table 7). More research on degradation rates of nitramines in soil and water is needed. The coupled model chain of the WRF-EMEP system and the fugacity model proved to be well suited for the prediction of yearly average ground-level air and drinking water concentrations of the sum of nitrosamines and

ACPD
14, 8633–8693, 2014

nitramines, the two major human health risk endpoints related to amine-based CO_2 capture.

This study for a full-scale post-combustion CO_2 capture plant based on amine technology shows that realistic emissions result in levels of the sum of nitrosamines and nitramines in ground-level air (0.6–10 $pg\,m^{-3}$) and drinking water (0.04–0.25 $ng\,L^{-1}$) downwind the CCP not exceeding the current safety guideline for human health by the Norwegian Environmental Directorate. A number of complicating factors could increase the health risk.

There are about 5000 large point sources (each emitting more than 0.1 million tonnes of CO_2 per year) for electricity power generation using fossil fuels worldwide which could be retrofitted using amine-based post-combustion. IPCC (2005) estimated that 30–60 % of the CO_2 emissions from electricity generation can be captured. National plans for building CCS infrastructure exist in EU Member States (e.g. in the UK), Canada, USA, Australia and China. Several post-combustion pilot plants and large scale demonstration plants are operative in Europe and in the USA (Esbjerg, Denmark; Karlshamn, Sweden; SCCS Edinburgh, Scotland, UK; Brindisi, Italy; Plant Barry, Alabama, USA); several full-scale plants or near full-scale plants are planned (Peterhead, Scotland, UK; ArcelorMittal Florange, France; Porto Tolle, Italy; WA Parish, Texas, USA; Samcheok City, South Korea); and one full-scale CCP to capture 1 million tonnes CO_2 per year is currently being build in Canada (Boundary Dam, Saskatchewan). A national or transnational plan on CCS infrastructure building might require the installation of several commercial scale CCP in one region, since most fossil fuel power plants are concentrated in the proximity of major industrial and urban regions. According to our study, building a CCP within a distance of 100–200 km downwind of an existing CCP will cause interferences, and amine emissions released from the neighbouring plant will add to the chemically produced nitrosamines and nitramines in the surroundings of the existing CCP. Such a scenario illustrates the possible complexity arising from increased use of post-combustion capture, and the need for advanced model tools such as the coupled WRF-EMEP and fugacity model system presented here.

ACPD
14, 8633–8693, 2014

Supplementary material related to this article is available online at http://www.atmos-chem-phys-discuss.net/14/8633/2014/acpd-14-8633-2014-supplement.pdf.

Acknowledgements. Special thanks to H. D. van der Gon for granting permission to make use of the fine scale emission data developed by TNO within the MACC project and to Bertrand Bessagnet (INERIS) for providing the emission data set. D. Tønnesen (NILU) is thanked for providing hourly air quality of Hamna and Leirvåg station. We thank the Notur infrastructure of UNINETT Sigma for allocation of CPU resources under project NN9257K. Evaluation of the WRF-EMEP model system with local meteorology and air quality observational data was performed in the framework of the technology qualification of amines for the CO_2 Capture Mongstad Project (CCM) funded by the Norwegian Government through Statoil Petroleum AS and Gassnova SF. We acknowledge financial support from the Research Council of Norway, Statoil Petroleum AS, Shell, and Vattenfall under project 199874 (ExSIRA, Part C). The authors also thank NILU for additional financial support.

References

Aas, W., Tsyro, S., Bieber, E., Bergström, R., Ceburnis, D., Ellermann, T., Fagerli, H., Frölich, M., Gehrig, R., Makkonen, U., Nemitz, E., Otjes, R., Perez, N., Perrino, C., Prévôt, A. S. H., Putaud, J.-P., Simpson, D., Spindler, G., Vana, M., and Yttri, K. E.: Lessons learnt from the first EMEP intensive measurement periods, Atmos. Chem. Phys., 12, 8073–8094, doi:10.5194/acp-12-8073-2012, 2012. 8642

Angove, D., Azzi, M., Tibbett, A., and Campbell, I.: An investigation into the photochemistry of monoethanolamine (MEA) in NO_x. in: Recent Advances in Post-Combustion CO_2 Capture Chemistry, ACS Symposium Series, Washington, DC, vol. 1097, chap. 14, 265–273, 2012. 8635

Berge, E. and Jakobsen, H. A.: A regional scale multi-layer model for the calculation of long-term transport and deposition of air pollution in Europe, Tellus, 50, 205–223, 1998. 8647

Briggs, G. A.: Plume Rise, US Atomic Energy Commission, Springfield, USA, 1969. 8643

ACPD
14, 8633–8693, 2014

Briggs, G. A.: Some recent analyses of plume rise observation, in: Proceedings of the Second International Clean Air Congress, edited by: Englund, H. M. and Berry, W. T., Academic Press, Washington, USA, 6–11 December , 1970, 1029–1032, 1971. 8643

Briggs, G. A.: Plume rise predictions, in: Lectures on Air Pollution and Environmental Impact Analysis, edited by: Haugen, D. A., Amer. Meteor. Soc., Boston, MA, 59–111, 1975. 8643

California EPA: Public Health Goal for N-nitrosodimethylamine in Drinking Water, California Environmental Protection Agency, Pesticide and Environmental Toxicology Branch, available at: http://oehha.ca.gov/water/phg/pdf/122206NDMAphg.pdf (last access: 10 December 2013), 2006. 8636

Colette, A., Granier, C., Hodnebrog, Ø., Jakobs, H., Maurizi, A., Nyiri, A., Bessagnet, B., D'Angiola, A., D'Isidoro, M., Gauss, M., Meleux, F., Memmesheimer, M., Mieville, A., Rouïl, L., Russo, F., Solberg, S., Stordal, F., and Tampieri, F.: Air quality trends in Europe over the past decade: a first multi-model assessment, Atmos. Chem. Phys., 11, 11657–11678, doi:10.5194/acp-11-11657-2011, 2011. 8640

Dai, N., Shah, A. D., Hu, L., Plewa, M. J., McKague, B., and Mitch, W. A.: Measurement of nitrosamine and nitramines formation from NO_x reactions with amines during amine-based carbon dioxide capture for postcombustion carbon sequestration, Environ. Sci. Technol., 46, 9793–9801, 2012. 8636

Dee, D. P., Uppala, S. M., Simmons, A. J., Berrisford, P., Poli, P., Kobayashi, S., Andrae, U., Balmaseda, M. A., Balsamo, G., Bauer, P., Bechtold, P., Beljaars, A. C. M., van de Berg, L., Bidlot, J., Bormann, N., Delsol, C., Dragani, R., Fuentes, M., Geer, A. J., Haimberger, L., Healy, S. B., Hersbach, H., Hólm, E. V., Isaksen, L., Kållberg, P., Köhler, M., Matricardi, M., McNally, A. P., Monge-Sanz, B. M., Morcrette, J.-J., Park, B.-K., Peubey, C., de Rosnay, P., Tavolato, C., Thépaut, J.-N., and Vitart, F.: The ERA-Interim reanalysis: configuration and performance of the data assimilation system, Q. J. Roy. Meteor. Soc., 137, 553–597, 2011. 8641

de Koeijer, G., Talstad, V. R., Nepstad, S., Tønnesen, D., Falk-Pedersen, O., Maree, Y., and Nielsen, C.: Health risk analysis of emissions to air from CO_2 Technology Center Mongstad, Int. J. Greenh. Gas Con., 18, 200–207, 2013. 8636, 8637, 8665, 8666

Drewes, J. E., Hoppe, C., and Jennings, T.: Fate and transport of n-nitrosamines under conditions simulating full-scale groundwater recharge operations, Water Environ. Res., 78, 2466–2473, doi:10.2175/106143006x115408, 2006. 8666

ACPD
14, 8633–8693, 2014

Fagerli, H. and Aas, W.: Trends of nitrogen in air and precipitation: model results and observations at EMEP sites in Europe, 1980–2003, Environ. Pollut., 154, 448–461, 2008. 8642
Fisher, B. E. A., Erbrink, J. J., Finardi, S., Jeannet, P., Joffre, S., Morselli, M. G., Pechinger, U., Seibert, P., and Thomson, D. J.: COST Action 710 – Final report, Harmonisation of the preprocessing of meteorological data for atmospheric dispersion models, EUR 18195, Office for Official Publications of the European Communities, Luxembourg, 431, 1998. 8644
Ge, X., Wexler, A. S., and Clegg, S. L.: Atmospheric amines – Part 2: Thermodynamic properties and gas/particle partitioning, Atmos. Environ., 45, 561–577, 2011. 8647
Goff, G. S. and Rochelle, G. T.: Monoethanolamine degradation: O_2 mass transfer effects under CO_2 capture conditions, Ind. Eng. Chem. Res., 43, 6400–6408, 2004. 8635
Hanna, S. R., Briggs, G. A., and Hosker Jr., R. P.: Handbook on Atmospheric Diffusion, edited by: Smith, J. S., DOE/TIC-11223, Technical Information Center, US Department of Energy, Springfield, USA, 1982. 8643
Holmes, N. S. and Morawska, L.: A review of dispersion modelling and its application to the dispersion of particles: an overview of different dispersion models available, Atmos. Environ., 40, 5902–5928, 2006. 8637
Högström, U.: Review of some basic characteristics of the atmospheric surface layer, Bound.-Lay. Meteorol., 78, 215–246, 1996. 8644
Hurley, P., Physick, W., and Luhar, A.: TAPM – a practical approach to prognostic meteorological and air pollution modelling, Environ. Modell. Softw., 20, 737–752, doi:10.1016/j.envsoft.2004.04.006, 2005. 8641, 8646
Hutchings, J. W., Ervens, B., Straub, D., and Herckes, P. N.: Nitrosodimethylamine occurrence, formation, and cycling in clouds and fogs, Environ. Sci. Technol., 41, 393–399, 2010. 8647
IPCC: Intergovernmental Panel on Climate Change (IPCC) Special Report on Carbon Dioxide Capture and Storage, Cambridge University Press, Cambridge, UK, 2005. 8669
Jonson, J. E., Simpson, D., Fagerli, H., and Solberg, S.: Can we explain the trends in European ozone levels?, Atmos. Chem. Phys., 6, 51–66, doi:10.5194/acp-6-51-2006, 2006. 8642
Kaplan, D. L. and Kaplan, A. M.: Biodegradation of n-nitrosodimethylamine in aqueous and soil systems, Appl. Environ. Microb., 50, 1077–1086, 1985. 8666
Karl, M., Wright, R. F., Berglen, T. F., and Denby, B.: Worst case scenario study to assess the environmental impact of amine emissions from a CO_2 capture plant, Int. J. Greenh. Gas Con., 5, 439–447, 2011. 8637, 8641, 8646, 8648, 8657, 8660, 8665

ACPD
14, 8633–8693, 2014

Karl, M., Dye, C., Schmidbauer, N., Wisthaler, A., Mikoviny, T., D'Anna, B., Müller, M., Borrás, E., Clemente, E., Muñoz, A., Porras, R., Ródenas, M., Vázquez, M., and Brauers, T.: Study of OH-initiated degradation of 2-aminoethanol, Atmos. Chem. Phys., 12, 1881–1901, doi:10.5194/acp-12-1881-2012, 2012. 8635, 8646

Kuenen, J., Denier van der Gon, H., Visschedijk, A., and van der Brugh, H.: High resolution European emission inventory for the years 2003–2007, TNO report TNO-060-UT-2011-00588, Utrecht, the Netherlands, 2011. 8642

Lazarou, Y. G., Kambanis, K. G., and Papagiannakopoulos, P.: Gas phase reactions of $(CH_3)_2N$ radicals with NO and NO_2, J. Phys. Chem., 98, 2110–2115, 1994.

Låg, M., Lindeman, B., Instanes, C., Brunborg, G., and Schwarze, P.: Health effects of amines and derivatives associated with CO_2 capture, Norwegian Institute of Public Health, available at: http://www.fhi.no/dokumenter/ca838717be.pdf (last access: 10 December 2013), 2011. 8635, 8636, 8639

Lee, D. and Wexler, A. S.: Atmospheric amines – Part 3: Photochemistry and toxicity, Atmos. Environ., 71, 95–103, doi:10.1016/j.atmosenv.2013.01.058, 2013. 8635

Mackay, D.: Multimedia Environmental Models: the Fugacity Approach, 2nd Edn., CRC press, Boca Raton, FL, 2001. 8642

Mackay, D., Di Guardo, A., Paterson, S., Kicsi, G., and Cowan, C. E.: Assessing the fate of new and existing chemicals: a five-stage process, Environ. Toxicol. Chem., 15, 1618–1626, 1996. 8643

MacLeod, M. and Mackay, D.: An assessment of the environmental fate and exposure of benzene and the chlorobenzenes in Canada, Chemosphere, 38, 1777–1796, 1999. 8643

MacLeod, M., Fraser, A. J., and Mackay, D.: Evaluating and expressing the propagation of uncertainty in chemical fate and bioaccumulation models, Environ. Toxicol. Chem., 21, 700–709, 2002. 8664

Malloy, Q. G. J., Li Qi, Warren, B., Cocker III, D. R., Erupe, M. E., and Silva, P. J.: Secondary organic aerosol formation from primary aliphatic amines with NO_3 radical, Atmos. Chem. Phys., 9, 2051–2060, doi:10.5194/acp-9-2051-2009, 2009. 8667

Nielsen, C. J., D'Anna, B., Dye, C., Graus, M., Karl, M., King, S., Musabila, M., Müller, M., Schmidbauer, N., Stenstrøm, Y., Wisthaler, A., and Pedersen, S.: Atmospheric chemistry of 2-aminoethanol (MEA), Energy Procedia, 4, 2245–2252, 2011. 8635, 8646, 8653

Nielsen, C. J., D'Anna, B., Bossi, R., Bunkan, A. J. C., Dithmer, L., Glasius, M., Hallquist, M., Hansen, A. M. K., Lutz, A., Salo, K., Maguta, M. M., Nguyen, Q., Mikoviny, T., Müller, M.,

ACPD
14, 8633–8693, 2014

Skov, H., Sarrasin, E., Stenstrøm, Y., Tang, Y., Westerlund, J., and Wisthaler, A.: Atmospheric Degradation of Amines (ADA): summary report from atmospheric chemistry studies of amines, nitrosamines, nitramines and amides, University of Oslo, Oslo, 2012a. 8645, 8646, 8652

Nielsen, C. J., Herrmann, H., and Weller, C.: Atmospheric chemistry and environmental impact of the use of amines in carbon capture and storage (CCS), Chem. Soc. Rev., 41, 6684–6704, 2012b. 8635, 8645, 8646, 8649, 8663

Norwegian Climate and Pollution Agency: Permit for Activities Pursuant to the Pollution Control Act for CO_2 Technology Centre Mongstad DA, available at: http://www.tcmda.com/Global/Dokumenter/Klif_TCM_Dischargepermit.pdf (last access: 10 December 2013), 2011. 8636

Onel, L., Blitz, M. A., and Seakins, P. W.: Direct determination of the rate coefficient for the reaction of OH radicals with monoethanol amine (MEA) from 296 to 510 K, J. Phys. Chem. Lett. 3, 853–856, 2012.

Owen, B., Edmunds, H. A., Carruthers, D. J., and Singles, R. J.: Prediction of total oxides of nitrogen and nitrogen dioxide concentrations in a large urban area using a new generation urban scale dispersion model with integral chemistry model, Atmos. Environ., 34, 397–406, 2000. 8637

Pitts, J. N., Grosjean, D., Vanmcauwenberghe, K., Schmidt, J. P., and Fitz, D. R.: Photooxidation of aliphatic amines under simulated atmospheric conditions: formation of nitrosamines, nitramines, amides, and photochemical oxidant, Environ. Sci. Technol., 12, 946–953, 1978. 8635

Plumlee, M. H. and Reinhard, M.: Photochemical attenuation of n-nitrosodimethylamine (NDMA) and other nitrosamines in surface water, Environ. Sci. Technol., 41, 6170–6176, 2007. 8666

Price, D. J.: Field and Smog Chamber Studies of Agricultural Emissions and Reaction Products, Master's thesis, All Graduate Theses and Dissertations, Paper 592, Utah State University, available at http://digitalcommons.usu.edu/etd/592 (last access: 10 December 2013), 2010. 8635, 8667, 8668

Rao, A. B. and Rubin, E. S.: A technical, economic, and environmental assessment of amine-based CO_2 capture technology for power plant greenhouse gas control, Environ. Sci. Technol., 36, 4467–4475, 2002. 8635

Reynolds, A. J., Verheyen, T. V., Adeloju, S. B., Meuleman, E., and Feron, P.: Towards commercial scale postcombustion capture of CO_2 with monoethanolamine solvent: key considera-

ACPD
14, 8633–8693, 2014

tions for solvent management and environmental impacts, Environ. Sci. Technol., 46, 3643–3654, 2012. 8636, 8666

Richardson, S. D., Plewa, M. J., Wagner, E. D., Schoeny, R., and DeMarini, D. M.: Occurrence, genotoxicity, and carcinogenicity of regulated and emerging disinfection by-products in drinking water: a review and roadmap for research, Mutat. Res.-Rev. Mutat, 636, 178–242, doi:10.1016/j.mrrev.2007.09.001, 2007. 8635

Rochelle, G. T.: Amine scrubbing for CO_2 capture, Science, 325, 1652–1653, 2009. 8634

Salo, K., Westerlund, J., Andersson, P. U., Nielsen, C. J., D'Anna, B., and Hallquist, M.: Thermal characterization of alkyl aminium nitrate nanoparticles, J. Phys. Chem. A, 115, 11671–11677, 2011. 8663

Saloranta, T. M., Armitage, J. M., Haario, H., Næs, K., Cousins, I. T., and Barton, D. N.: Modeling the effects and uncertainties of contaminated sediment remediation scenarios in a Norwegian Fjord by Markov chain Monte Carlo simulation, Environ. Sci. Technol., 42, 200–206, 2007. 8664

Simpson, D., Fagerli, H., Hellsten, S., Knulst, J. C., and Westling, O.: Comparison of modelled and monitored deposition fluxes of sulphur and nitrogen to ICP-forest sites in Europe, Biogeosciences, 3, 337–355, doi:10.5194/bg-3-337-2006, 2006. 8642

Simpson, D., Butterbach-Bahl, K., Fagerli, H., Kesik, M., Skiba, U., and Tang, S.: Deposition and emissions of reactive nitrogen over European forests: a modelling study, Atmos. Environ., 40, 5712–5726, 2006b.

Simpson, D., Benedictow, A., Berge, H., Bergström, R., Emberson, L. D., Fagerli, H., Flechard, C. R., Hayman, G. D., Gauss, M., Jonson, J. E., Jenkin, M. E., Nyíri, A., Richter, C., Semeena, V. S., Tsyro, S., Tuovinen, J.-P., Valdebenito, Á., and Wind, P.: The EMEP MSC-W chemical transport model – technical description, Atmos. Chem. Phys., 12, 7825–7865, doi:10.5194/acp-12-7825-2012, 2012. 8637, 8642, 8647, 8648

Skamarock, W. C. and Klemp, J. B.: A time-split nonhydrostatic atmospheric model for weather research and forecasting applications, J. Comput. Phys., 227, 3465–3485, doi:10.1016/j.jcp.2007.01.037, 2008. 8637

Skamarock, W. C., Klemp, J. B., Dudhia, J., Gill, D. O., Barker, D. M., Duda, M. G., Huang, X.-Y., Wang, W., and Powers, J. G.: A Description of the Advanced Research WRF Version 3, NCAR Technical note, NCAR/TN-475+STR, available at: http://www.mmm.ucar.edu/wrf/users/docs/arw_v3.pdf (last access: 10 December 2013), 2008. 8640, 8641

ACPD
14, 8633–8693, 2014

Solberg, S. and Svendby, T.: Development of a nested WRF/EMEP modelling system at NILU, in: Transboundary acidification, eutrophication and ground level ozone in Europe in 2010, edited by: Fagerli, H., Gauss, M., Benedictow, A., Jonson, J. E., Nyíri, A., Schulz, M., Simpson, D., Steensen, B. M., Tsyro, S., Valdebenito, A., Wind, P., Shamsudheen, S. V., Aas, W., Hjelbrekke, A.-G., Mareckova, K., Wankmuller, R., Solberg, S., Svendby, T., Vieno, M., Thunis, P., Cuvelier, K., Koffi, B., and Bergtström, R., Norwegian Meteorological Institute – MSC-W (EMEP status report 1/2012), Oslo, 81–89, 2012. 8640

Strazisar, B. R., Anderson, R. R., and White, C. M.: Degradation pathways of monoethanolamine in a CO_2 capture facility, Energ. Fuel., 17, 1034–1039, 2003. 8635

Tang, Y., Hanrath, M., and Nielsen, C. J.: Do primary nitrosamines form and exist in the gas phase? A computational study of CH_3NHNO and $(CH_3)_2NNO$, Phys. Chem. Chem. Phys., 14, 16365–16370, 2012. 8646

Tønnesen, D., Dye, C., and Bøhler, T.: Baseline study on air and precipitation quality for CO_2 Technology Centre Mongstad, Norwegian Institute for Air Research, NILU OR 73/2011, Kjeller, Norway, 2011. 8666

US EPA: Estimation Programs Interface Suite for Microsoft Windows, v 4.00, United States Environmental Protection Agency, Washington, DC, USA, available at: http://www.epa.gov/opptintr/exposure/pubs/episuite.htm (last access: 10 December 2013), 2012. 8643

Verwer, J. and Simpson, D.: Explicit methods for stiff ODEs from atmospheric chemistry, Appl. Numer. Math., 18, 413–430, 1995. 8642

Verwer, J. G., Blom, J. G., and Hundsdorfer, W.: An implicit explicit approach for atmospheric transport-chemistry problems, Appl. Numer. Math., 20, 191–209, 1996. 8642

Vieno, M., Dore, A. J., Wind, P., Di Marco, C., Nemitz, E., Phillips, G., Tarrason, L., and Sutton, M. A.: Application of the EMEP Unified Model to the UK with a Horizontal Resolution of $5 \times 5\,km^2$, in: Atmospheric Ammonia – Detecting Emission Changes and Environmental Impacts, edited by: Sutton, M. A., Reid, S., and Baker, S. M. H., Springer, Berlin, Heidelberg, Germany, 367–372, 2009. 8640

Vieno, M., Dore, A. J., Stevenson, D. S., Doherty, R., Heal, M. R., Reis, S., Hallsworth, S., Tarrason, L., Wind, P., Fowler, D., Simpson, D., and Sutton, M. A.: Modelling surface ozone during the 2003 heat-wave in the UK, Atmos. Chem. Phys., 10, 7963–7978, doi:10.5194/acp-10-7963-2010, 2010. 8640

Wieringa, J.: Updating the Davenport roughness classification, J. Wind Eng. Ind. Aerod., 41–44, 357–368, 1992. 8644

ACPD
14, 8633–8693, 2014

Wolke, R., Knoth, O., Hellmuth, O., Schroder, W., and Renner, E.: The parallel model system LM/MUSCAT for chemistry transport simulations: coupling scheme, parallelization and applications, Adv. Par. Com., 13, 363–369, 2004. 8652

Yang, W. C., Gan, J., Liu, W. P., and Green, R.: Degradation of n-nitrosodimethylamine (NDMA) in landscape soils, J. Environ. Qual., 34, 336–341, 2005. 8666

Zhou, Q. L., McCraven, S., Garcia, J., Gasca, M., Johnson, T. A., and Motzer, W. E.: Field evidence of biodegradation of n-nitrosodimethylamine (NDMA) in groundwater with incidental and active recycled water recharge, Water Res., 43, 793–805, doi:10.1016/j.watres.2008.11.011, 2009. 8666

ACPD
14, 8633–8693, 2014

Table 1. Stack data and emission data of the CCP at Mongstad applied in this study. Data sources: Rao and Rubin (2002), Karl et al. (2011). It is stressed that the stack design and emissions of the CCP does not represent any existing post-combustion plant.

Stack parameter		Value
Geographic coordinates (lat|lon)		60.809° N|5.036° E
Stack height H_s	(m)	60.0
Stack diameter D	(m)	7.14
Exhaust gas exit temperature	(°C)	40.0
Exhaust gas exit velocity Vs	($m\,s^{-1}$)	10.0
Emission MEA	($g\,s^{-1}$)	1.2684
Emission DEYA	($g\,s^{-1}$)	0.1585
Emission NO	($g\,s^{-1}$)	4.2174
Emission NO_2	($g\,s^{-1}$)	0.2220

ACPD
14, 8633–8693, 2014

Table 2. Atmospheric photo-oxidation scheme for MEA (primary amine RNH_2) and DEYA (secondary amine, RR′NH) implemented in the EMEP model. Branching of the amine chemistry scheme, rate constants (k) and photolysis frequency (j) for nitrosamine photolysis were adopted with modifications from Nielsen et al. (2012a). The branch leading to nitrosamines was deactivated for MEA; instead the imine of MEA is formed directly in reaction with NO.

No.	Reaction Educts		Reaction Products	Rate constant
1	$RNH_2 + OH$	→	$RNH\cdot$	k_{1a}(MEA)
2	$RNH\cdot + NO$	→	$R{=}NH + HONO$	k_2(MEA)
3	$RNH\cdot + NO_2$	→	$RNHNO_2$	k_3(MEA)
4	$RNH\cdot + NO_2$	→	$R{=}NH + HONO$	k_4(MEA)
5	$RNH\cdot + O_2$	→	$R{=}NH + HO_2$	k_5(MEA)
6	$RNHNO_2 + OH$	→	$R(=O)NHNO_2 + HO_2$	k_6(MEA)
7	$RNH_2 + NO_3$	→	$RNH\cdot$	k_7(MEA)[g]
8	RR′NH + OH	→	RR′N·	k_{1a}(DEYA)
9	RR′N· + NO	→	RNR′NO	k_2(DEYA)
10	RR′N· + NO_2	→	0.5 RNR′NO_2 + 0.5 R=NR′ + 0.5 HONO	k_3(DEYA)
11	RR′N· + O_2	→	$R{=}NH + HO_2$	k_5(DEYA)
12	RNR′NO_2 + OH	→	$R(=O)NR'NO_2 + HO_2$	k_6(DEYA)
13	RNR′NO + hν	→	RR′N· + NO	j_1(DEYA)

Comp.	k_1 [a,b]	k_2 [a,d]	k_6 [a,d]	k_4 [a]	k_{1a}/k_1 [d]	k_2/k_3 [d,f]	k_4/k_3 [d,f]	k_5/k_3 [d,f]	$j_1/j_{(NO_2)}$ [d]
MEA	7.61×10^{-11} [c]	8.32×10^{-14} [e]	3.5×10^{-12}	7.0×10^{-14}	0.08	0.26	0.22	3.9×10^{-7}	–
DEYA	7.40×10^{-11} [c]	2.24×10^{-13}	4.6×10^{-12}	0.0	0.60	0.70	0.0	1.1×10^{-6}	0.3

[a] Unit: $cm^3\,molecule^{-1}\,s^{-1}$, photolysis rates in units s^{-1}.
[b] Rate constant k_1 is the overall rate constant of the OH + amine reaction.
[c] Reference: Onel et al. (2012).
[d] Reference: Nielsen et al. (2012a).
[e] Reaction forms imine instead of nitrosamine.
[f] Rate constant $k_3 = 3.20 \times 10^{-13}\,cm^3\,molecule^{-1}\,s^{-1}$. Reference: Lazarou et al. (1994).
[g] Rate constant $k_7 = 1.5 \times 10^{-13}\,cm^3\,molecule^{-1}\,s^{-1}$. Reference: Karl et al. (2012). Reaction MEA + NO_3 was only taken into account in the sensitivity test case KNO3M (Sect. 2.7).

ACPD
14, 8633–8693, 2014

Table 3. Summary of model aspects included in the sensitivity analysis of the EMEP model. Changes of chemical/physiochemical properties were only done for MEA and MEA-nitramine. Rate constants given in unit $cm^3\,molecule^{-1}\,s^{-1}$.

Model aspect	Case name	Baseline	Alternate
Vertical emission profile	PLUME	NILU plume	PVDI plume
Rate constant k(MEA + OH)	KOHM	7.6×10^{-11}	9.2×10^{-11}
Rate constant k(MEA + NO_3)	KNO3M	0.0	1.5×10^{-13}
Branching ratio H-abstr. at NH_2-group	YIELD	0.08	0.16
Rate constant k(MEA–nitramine + OH)	KNIM	1.48×10^{-11}	3.5×10^{-12}
Aqueous phase partitioning	AQP	no	yes
Wet deposition	WDEP	as HNO_3	as SO_2

ACPD
14, 8633–8693, 2014

Table 4. Summary of model aspects included in the sensitivity analysis of the fugacity model. Each parameter was changed independently. The degradation rates (expressed as lifetime in days) refer to the values for the compartments air/soil/water/sediment.

Model aspect	Case name	Baseline	Alternate
Hydrology – residence time through lake depth	HydDep	10 m	5 m 20 m
Hydrology – residence time through lake area	HydArea	0.16 km^2	0.08 km^2 0.32 km^2
Soil – depth	SoilDep	0.1 m	0.05 m 0.2 m
Chemistry – fraction organic carbon in soil	ChemSoil	0.014	0.007 0.028
Chemistry – fraction org. carbon in susp. sediments	ChemSed	0.14	0.07 0.28
Degredation rates nitramines	DegRateMNA	8.5/30/15/135 days	8.5/4.6/2.3/4.6 days
Degredation rates nitrosamines	DegRateNDMA	4.2/38/23/207 days	4.2/5/0.7/2.7 days

ACPD
14, 8633–8693, 2014

Table 5. Worst case for the atmospheric fate and worst case for the soil-water-sediment fate and the respective baseline cases. Worst cases were designed based on results from the parameter variation cases. For explanations on the model aspects see Tables 3 and 4.

Atmospheric fate			Soil-water-sediment fate		
Model aspect	Baseline	Worst Case	Model aspect	Baseline	Worst Case
Vertical emission profile	NILU Plume	NILU Plume	Residence time, lake depth	10 m	5 m
k(MEA + OH)	7.6×10^{-11}	9.2×10^{-11}	Residence time, lake area	0.16 km^2	0.08 km^2
k(MEA + NO_3)	0.0	1.5×10^{-13}	Soil – depth	0.1 m	0.05 m
Branching ratio at NH_2-group	0.08	0.16	Chemistry, fraction OC soil	0.014	0.007
k(MEA–nitramine + OH)	1.48×10^{-11}	3.5×10^{-12}	Chemistry, fraction OC susp. sediment	0.14	0.14
Aqueous phase partitioning	no	no	Degradation rate, nitramines	8.5/30/15/ 135 days	8.5/30/15/ 135 days
Wet deposition	HNO_3	HNO_3	Degradation rate, nitrosamines	4.2/38/23/ 207 days	4.2/38/23/ 207 days

ACPD
14, 8633–8693, 2014

Table 6. Overview of results from the simulation runs. Maximum surface air concentration of amines (MEA + DEYA), sum of nitrosamines and nitramines, wet deposition flux, and drinking water concentration of sum nitrosamines and nitramines in the study area 40 km × 40 km around CCP Mongstad. The relative change (in %) of the max. total deposition of sum nitrosamines and nitramines and the relative change (in %) of the max. drinking water sum concentration compared to the baseline case are also shown. Concentration sum and flux sum refer to the sum of all nitrosamines and nitramines. Maximum total deposition computed by the EMEP model was used to determine maximum drinking water concentration with the fugacity level III model. Dry and wet deposition fluxes were taken from the EMEP grid cell with the maximum total deposition. Safety limits set by the Norwegian Environmental Directorate are given in the last column.

	BASE	PLUME	KOHM	KNO3M	YIELD	KNIM	AQP	WDEP	Worst	Safety limit
Max. surface air concentration amines ($ng\,m^{-3}$)	64.9	25.9	64.8	64.7	64.9	64.9	65.0	65.5	64.7	–
Max. surface air concentration sum ($pg\,m^{-3}$)	3.7	0.6	4.2	5.6	6.5	3.7	1.4	3.7	9.6	300.0
Max. total deposition flux sum ($\mu g\,m^{-2}$)	1.37	1.16	1.57	2.27	2.45	1.37	0.67	1.08	3.79	–
Wet deposition flux sum at max. location ($\mu g\,m^{-2}$)	0.41	1.05	0.47	0.81	0.73	0.41	0.57	0.12	1.45	–
Dry deposition flux sum at max. location ($\mu g\,m^{-2}$)	0.96	0.11	1.10	1.46	1.72	0.96	0.10	0.96	2.34	–
Rel. change of max. total deposition flux sum (%)	0	−15	+15	+66	+79	< 1	−51	−21	+176	–
Max. drinking water concentration sum ($ng\,L^{-1}$)	0.08	0.07	0.10	0.13	0.15	0.08	0.04	0.07	0.22	4.0
Rel. change of max. drinking water conc. sum (%)	0	−19	+15	+60	+75	< 1	−52	−21	+168	–

ACPD
14, 8633–8693, 2014

Table 7. Results of the fugacity model given variations in several parameters. Shown are simulated maximum concentrations sum of nitrosamine and nitramines (ng L^{-1}) in a generic lake. For each case (see Table 4) the predicted sum of contaminants are given for the high (top) and low (bottom) parameter value settings or for the single changed parameter set (degradation rates and worst case). Case "Worst" uses the worst case parameters for soil-water-sediment fate (Table 5). All fugacity model calculations are based on the WRF-EMEP baseline case (BASE) results.

Base	Hyd Dep	Hyd Area	Soil Dep	Chem Soil	Chem Sed	Degrate MNA	Degrate NDMA	Worst	Safety limit
0.082	0.146 0.044	0.145 0.044	0.087 0.074	0.082 0.082	0.082 0.082	0.009	0.074	0.253	4.0

ACPD
14, 8633–8693, 2014

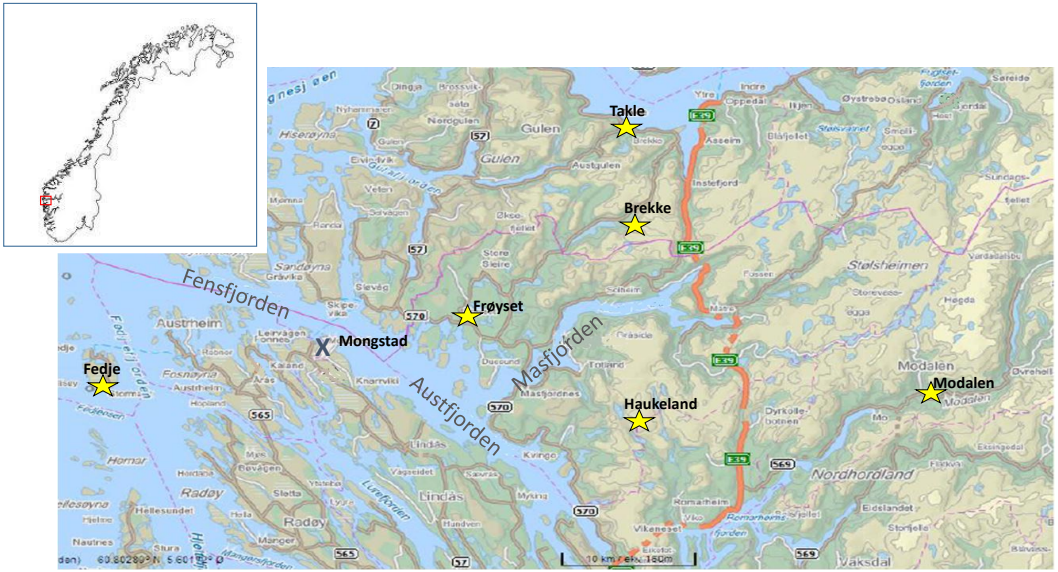

Fig. 1. Topographic map of the study area. The industrial area at Mongstad is indicated by a blue X. Meteorological stations are shown by yellow stars. Inset in the upper left corner shows the location of the study area in Norway.

ACPD
14, 8633–8693, 2014

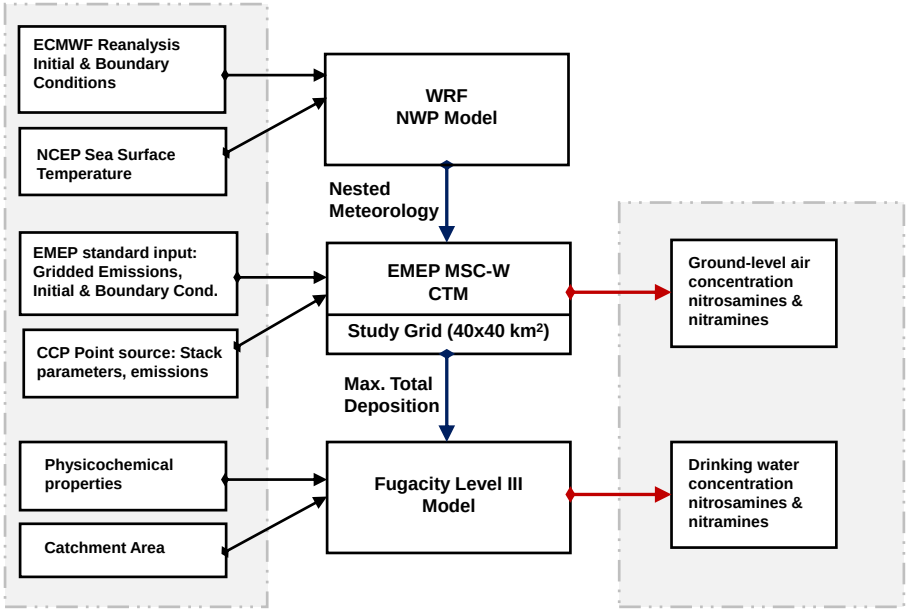

Fig. 2. Diagram of the WRF-EMEP model system coupled with a fugacity level III model for application in this study. Left column: standard input data and study-specific input data for the 3 models; middle column: WRF, EMEP, and fugacity model; right column: model output for comparison to the respective environmental safety limits.

ACPD
14, 8633–8693, 2014

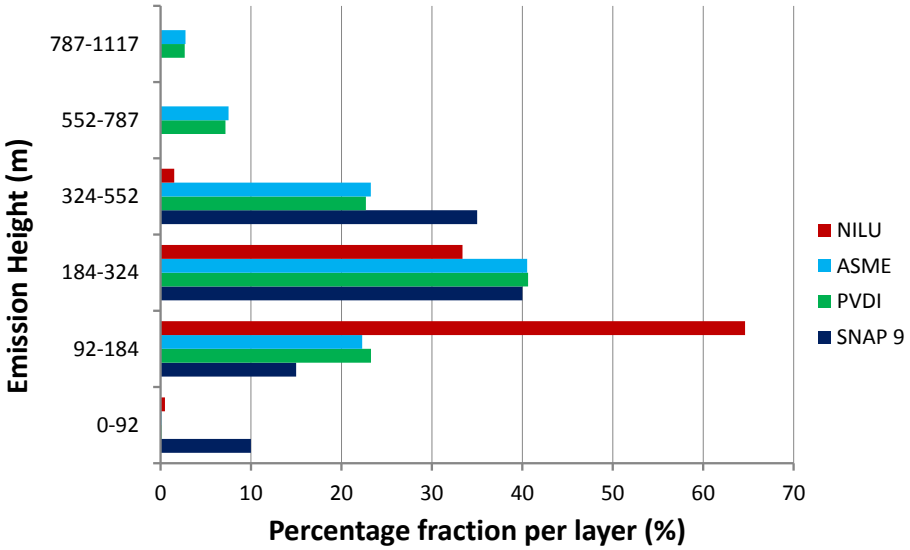

Fig. 3. Vertical emission profile of the CCP point source for SNAP category 9 and for the options "NILU Plume", "ASME Plume" and "PVDI Plume" in WRF-EMEP calculated for July 2007, using stack parameters of Table 1. Percentage fractions in the six layers for "NILU Plume", "ASME Plume" and "PVDI Plume" are based on 8928 online calculated profiles.

ACPD
14, 8633–8693, 2014

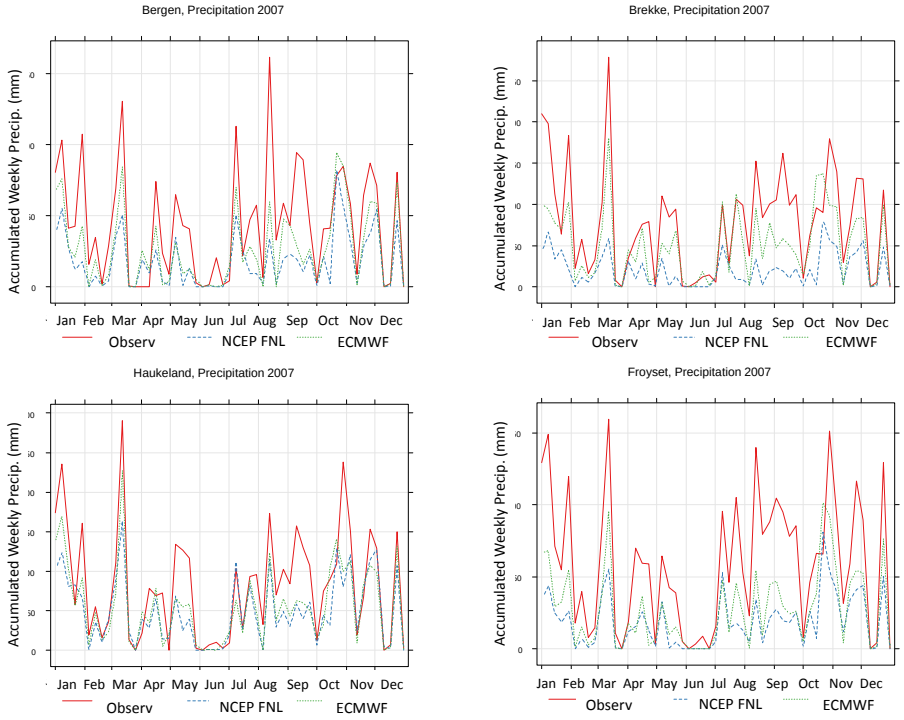

Fig. 4. Comparison of precipitation amount (mm) time series for 2007 at Bergen, Brekke, Haukeland, and Frøyset based on weekly intervals from observation (red line), WRF model with ECMWF data (green dashed line) and WRF model with NCEP FNL data (blue dashed line).

ACPD
14, 8633–8693, 2014

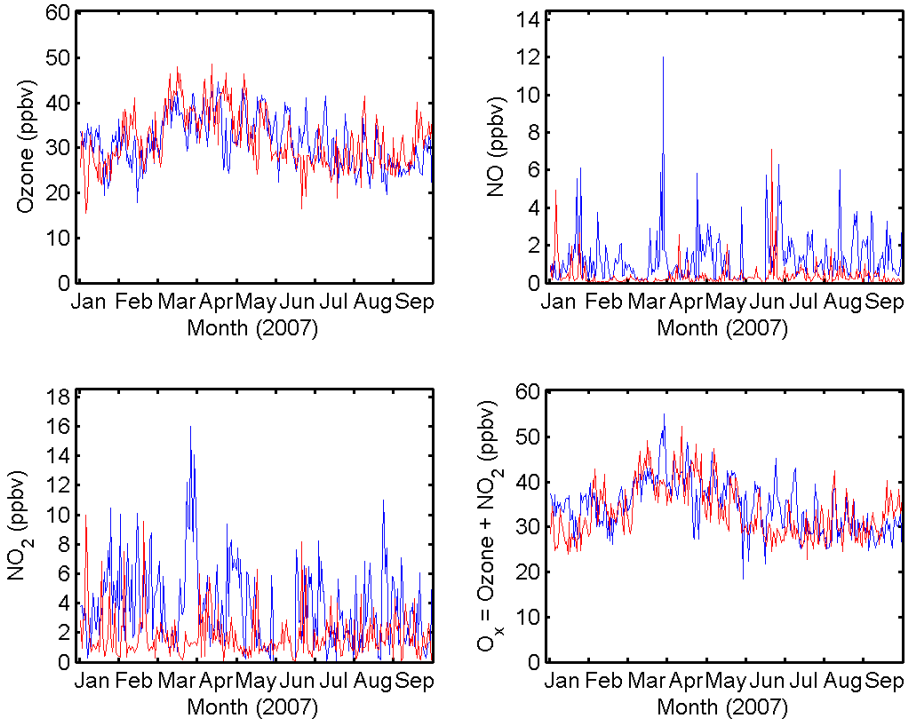

Fig. 5. Comparison of air quality data (daily averages of O_3, NO, NO_2, O_x) at Hamna, January–September 2007. Modelled ground air mixing ratios (ppbv) with WRF-EMEP (red lines) and monitored mixing ratios (ppbv; blue lines). Data gap in observed NO and NO_2 data from 28 May to 14 June.

ACPD
14, 8633–8693, 2014

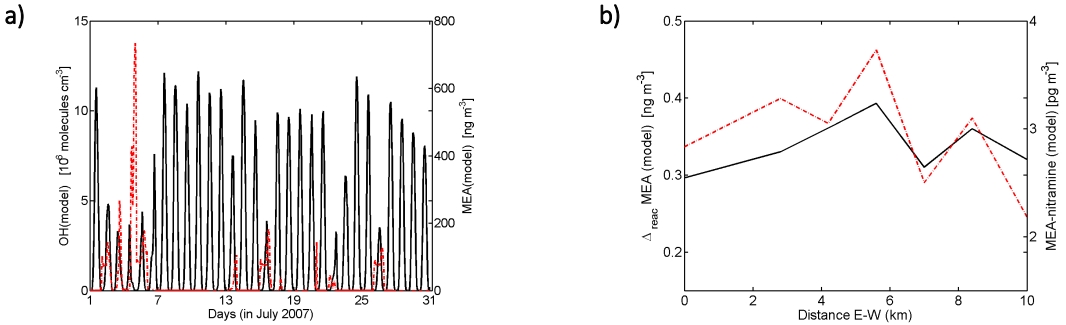

Fig. 6. Photochemical production of MEA-nitramine in WRF-EMEP: **(a)** modelled gas phase concentration of OH (black line) and MEA (red dash-dotted line) at Mongstad in July 2007, and **(b)** modelled yearly averaged reacted amount (black line) of the primary amine MEA (Δ_{reac}; calculated as concentration difference between MEA and an inert tracer emitted with the same amount of 1.27 g s^{-1}) and air concentration of MEA-nitramine (red dash-dotted line) as function of distance from the CCP Mongstad in E–W direction.

ACPD
14, 8633–8693, 2014

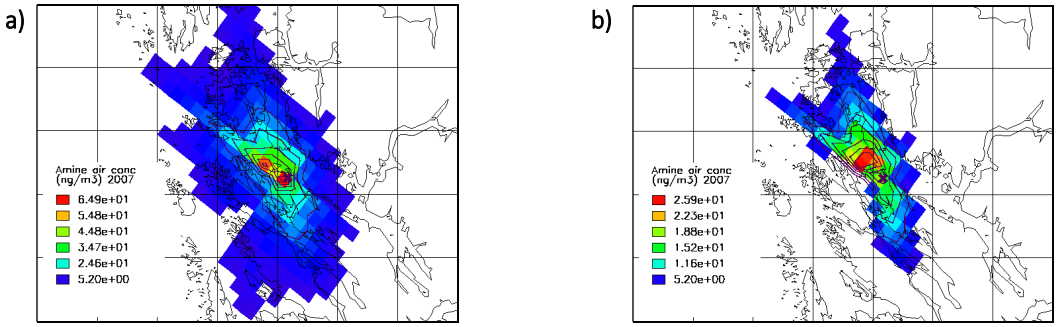

Fig. 7. Spatial distribution of the annual average (year 2007) ground-level air concentration of amines (sum of MEA and DEYA, in $ng\,m^{-3}$) computed by WRF-EMEP in the **(a)** baseline case (BASE), and in **(b)** case PLUME which uses the "PVDI Plume" parameterization. Different concentration scales are used for better clarity of the dispersion patterns. Values below the smallest legend entry (here $5.2\,ng\,m^{-3}$) are not shown. The location of CCP Mongstad is marked by a purple X. The grid cells divided by black lines illustrate an extent of 10 km × 10 km.

ACPD
14, 8633–8693, 2014

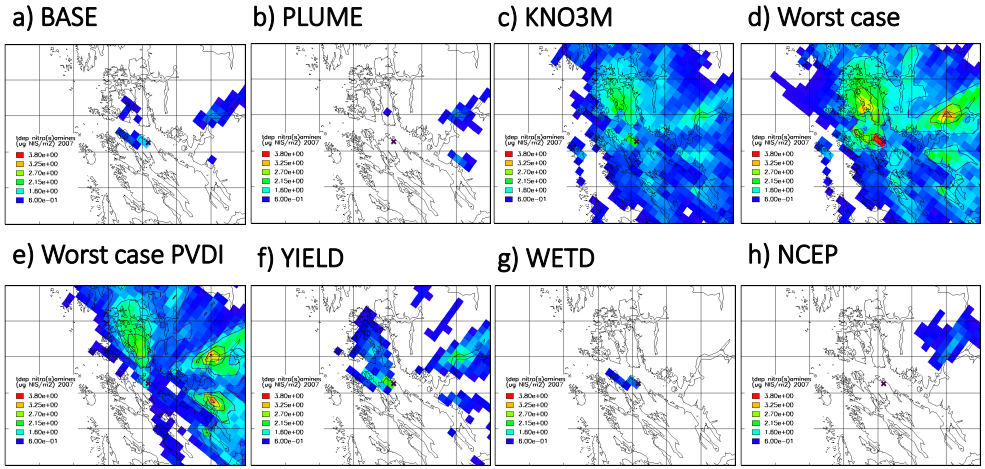

Fig. 8. Total deposition flux (dry and wet deposition) of the sum of nitrosamines and nitramines (in $\mu g\,m^{-2}$). Spatial distribution of the annual (year 2007) computed by WRF-EMEP in the **(a)** baseline case (BASE), **(b)** case PLUME using the "PVDI Plume" parameterization, **(c)** case KNO3M which includes the reaction of MEA with NO_3 radicals, **(d)** worst case using the parameter values given in Table 5, **(e)** worst case with "PVDI Plume" instead of "NILU Plume", **(f)** case YIELD, **(g)** case WETD, and **(h)** baseline case using NCEP FNL meteorological data. Values below the smallest legend entry are not shown. The location of CCP Mongstad is marked by a purple X. The grid cells divided by black lines illustrate an extent of 10 km × 10 km. All plots have the same concentration scale.

ACPD
14, 8633–8693, 2014

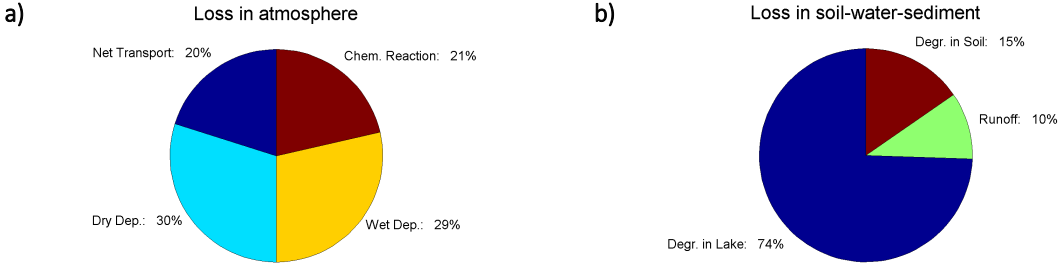

Fig. 9. Percentage removal pathways of the sum of nitrosamines and nitramines **(a)** in the atmosphere in the 200 km × 200 km inner domain from the WRF-EMEP simulation and **(b)** in the soil-water-sediment compartments at the location of maximum deposition calculated by the fugacity level III model. Results are from the baseline simulation.

ACPD
14, 8633–8693, 2014